2021

Spitzer'S Last Look At Extragalactic Explosions: Long-Term Evolution Of Interacting Supernovae

T Szalai
szaszi@titan.physx.u-szeged.hu

O D. Fox

R G. Arendt

E Dwek

T Szalai

See next page for additional authors

Recommended Citation

Szalai, T., Fox, O. D., Arendt, R. G., Dwek, E., Szalai, T., Clayton, G. C., Filippenko, A. V., Johansson, J., Kelly, P. L., Krafton, K., Marston, A. P., Mauerhan, J. C., Van, D. y., & SD. (2021). Spitzer'S Last Look At Extragalactic Explosions: Long-Term Evolution Of Interacting Supernovae. *Astrophysical Journal, 919* (1) https://doi.org/10.3847/1538-4357/ac0e2b

The Astrophysical Journal, 919:17 (19pp), 2021 September 20 https://doi.org/10.3847/1538-4357/ac0e2b

Spitzer's Last Look at Extragalactic Explosions: Long-term Evolution of Interacting Supernovae

Tamás Szalai[1,2], Ori D. Fox[3], Richard G. Arendt[4,5], Eli Dwek[4], Jennifer E. Andrews[6], Geoffrey C. Clayton[7], Alexei V. Filippenko[8,9], Joel Johansson[10], Patrick L. Kelly[11], Kelsie Krafton[7], A. P. Marston[12], Jon C. Mauerhan[13], and Schuyler D. Van Dyk[14]

[1] Department of Optics and Quantum Electronics, Institute of Physics, University of Szeged, Dóm tér 9, Szeged, 6720 Hungary; szaszi@titan.physx.u-szeged.hu
[2] Konkoly Observatory, Research Centre for Astronomy and Earth Sciences, H-1121 Budapest, Konkoly Thege Miklós út 15-17, Hungary
[3] Space Telescope Science Institute, 3700 San Martin Drive, Baltimore, MD 21218, USA
[4] Code 665, NASA/GSFC, 8800 Greenbelt Road, Greenbelt, MD 20771, USA
[5] CRESST II/UMBC, USA
[6] Steward Observatory, University of Arizona, 933 North Cherry Avenue, Tucson, AZ 85721-0065, USA
[7] Department of Physics & Astronomy, Louisiana State University, Baton Rouge, LA 70803, USA
[8] Department of Astronomy, University of California, Berkeley, CA 94720-3411, USA
[9] Miller Institute for Basic Research in Science, University of California, Berkeley, CA 94720, USA
[10] Oskar Klein Centre, Department of Physics, Stockholm University, SE-106 91 Stockholm, Sweden
[11] School of Physics and Astronomy, University of Minnesota, 116 Church Street SE, Minneapolis, MN 55455, USA
[12] ESA/JWST, Space Telescope Science Institute, 3700 San Martin Drive, Baltimore, MD 21218, USA
[13] The Aerospace Corporation, 2310 E. El Segundo Blvd., El Segundo, CA 90245, USA
[14] Caltech/IPAC, Mailcode 100-22, 1200 E. California Blvd., Pasadena, CA 91125, USA
Received 2021 May 12; revised 2021 June 22; accepted 2021 June 22; published 2021 September 17

Abstract

Here we present new, yet final, mid-infrared (mid-IR) data for supernovae (SNe) based on measurements with the Spitzer Space Telescope. Comparing our recent 3.6 and 4.5 μm photometry with previously published mid-IR and further multiwavelength data sets, we were able to draw some conclusions about the origin and heating mechanism of the dust in these SNe or in their environments, as well as about possible connection with circumstellar matter (CSM) originating from pre-explosion mass-loss events in the progenitor stars. We also present new results regarding both certain SN classes and single objects. We highlight the mid-IR homogeneity of SNe Ia-CSM, which may be a hint of their common progenitor type and of their basically uniform circumstellar environments. Regarding single objects, it is worth highlighting the late-time interacting Type Ib SNe 2003gk and 2004dk, for which we present the first-ever mid-IR data, which seem to be consistent with clues of ongoing CSM interaction detected in other wavelength ranges. Our current study suggests that long-term mid-IR follow-up observations play a key role in a better understanding of both pre- and post-explosion processes in SNe and their environments. While Spitzer is not available anymore, the expected unique data from the James Webb Space Telescope, as well as long-term near-IR follow-up observations of dusty SNe, can bring us closer to the hidden details of this topic.

Unified Astronomy Thesaurus concepts: Supernovae (1668); Infrared astronomy (786); Infrared telescopes (794); Circumstellar matter (241); Circumstellar dust (236)

1. Introduction

Supernovae (SNe) are the final explosions of either evolved massive stars or white dwarfs (WDs) located in binary systems. These events are important astrophysical laboratories for studying not just the details of the cataclysmic endings of stars, but also the preceding stellar evolution processes and the effect of SNe on their surrounding environments. Either early-time (so-called "flash") spectroscopy, or long-term (multi-channel) follow-up observations of the SN ejecta and their interaction with the surrounding circumstellar medium (CSM) can provide important details about the pre-explosion mass-loss history of the progenitors and the physics of shock waves. Beyond that, late-time observations can allow us to reveal the signs of special astrophysical processes that may take place during the interaction (e.g., ionization and recombination of the gas, or heating/formation of dust grains).

Both the timescale and degree of ejecta–CSM interaction vary among explosions and, specifically, among SN type and subclass. Type IIn SNe were the original class of SNe exhibiting clear signatures of interaction between the ejecta and dense, nearby CSM (e.g., relatively narrow optical emission lines denoted by "n" in SNe IIn, as well as strong X-ray and radio emission) within days of the explosion (Schlegel 1990). While the origin of SNe IIn is generally explained with core-collapse (CC) explosions of massive stars into previously expelled H-rich environments, similar phenomena can happen in the presence of a dense He-rich CSM (called SNe Ibn). Additionally, progressively more "normal" CC or thermonuclear SNe (i.e., exploding WDs) are found to eventually start producing detectable signs of interaction (occurring in CSM shells at larger distances from the explosion site); see, e.g., Vinkó et al. (2017), as well as the recent reviews of Chevalier & Fransson (2017) and Smith (2017).

Existing ground-based transient surveys ensure the optical monitoring of hundreds of SNe every year; however, these observations focus mostly on the "early" ($\lesssim$3 yr) phases of the objects. Late-time observations (either optical or at other wavelengths) are mostly occasional because they require large-aperture or space telescopes. Mid-infrared (mid-IR) observations at late times, in particular, offer several advantages over optical SN observations: increased sensitivity to the ejecta as they expand and cool, less impact from interstellar extinction, and coverage of atomic and molecular

emission lines generated by shocked, cooling gas (see, e.g., Reach et al. 2006). Perhaps most important, mid-IR observations are also sensitive to warm dust in the SN environment.

The origin and heating mechanism of the dust, however, are not always obvious, because the dust may be newly formed or pre-existing in the CSM. Newly condensed dust may form either in the ejecta or in a cool dense shell (CDS) between the shocked CSM and shocked ejecta where material cools (see, e.g., Pozzo et al. 2004; Mattila et al. 2008). Pre-existing dust may be radiatively heated by the peak SN luminosity or by the radiation from the shock breakout (e.g., Dwek & Arendt 2008), or by energetic photons generated during late-time CSM interaction, thereby forming an IR echo (see, e.g., Bode & Evans 1980; Dwek 1983; Graham & Meikle 1986; Sugerman 2003; Kotak et al. 2009). In this case, the dust is a useful probe of the CSM characteristics and the pre-SN mass loss from either the progenitor or companion star (see, e.g., Gall et al. 2011, for a review).

In the last 1.5 decades, the Spitzer Space Telescope (hereafter Spitzer)—especially its InfraRed Array Camera (IRAC) detector (Fazio et al. 2004)—was the primary source of mid-IR SN observations. Between 2003 and 2009, during the cryogenic (or Cold Mission) phase, only a moderate number ($<$50) of nearby SNe were targeted by Spitzer. After 2009, by this time with post-cryo (Warm Mission) Spitzer (with the availability of the two shortest-wavelength IRAC channels at 3.6 and 4.5 μm), two large surveys contributed to this surge: a program aimed to observe a large sample of Type IIn SNe ($\sim$70 observed SN sites, 13 detected targets; see Fox et al. 2011, 2013), and Spitzer Infrared Intensive Transients Survey (SPIRITS), a systematic mid-IR study of nearby ($\lesssim$20 Mpc) galaxies. SPIRITS has resulted in the detection of $\sim$50 SNe of various types (Tinyanont et al. 2016; Kasliwal et al. 2017; Jencson et al. 2019), including obscured SNe missed by previous optical surveys (Jencson et al. 2017, 2018, 2019), as well as some other transients showing unusual IR behavior (Kasliwal et al. 2017). Beyond these studies and a number of single-object papers, further broader studies were also presented regarding the mid-IR behavior of SNe II-P (Szalai & Vinkó 2013) and SNe Ia (Johansson et al. 2017).

Most recently, some of us (Szalai et al. 2019a) published a comprehensive analysis of the largest mid-IR data set of SNe ever studied (Spitzer data for $\sim$1100 SN sites including 120 positive detections). This sample—including all previously published data on most SNe discovered up to 2015, as well as many further objects that appeared on nontargeted Spitzer images—allowed an in-depth analysis to constrain the origin and heating mechanism of the dust in each SN type, and to perform preliminary statistics on their long-term mid-IR evolution. One of the main findings of this study was that subtypes of CC SNe tend to fill their own regions of phase space (IR luminosity, dust temperature, dust mass), while in thermonuclear SNe, there is a huge gap in late-time mid-IR properties of the few strongly interacting SNe and the only slightly detected or undetected objects. Furthermore, SNe IIn and other strongly interacting SNe remain bright for several years after explosion in the mid-IR, probably due to radiation from a large amount ($\gtrsim 10^{-3}\,M_{\odot}$) of pre-existing, radiatively heated dust grains.

Up to its decommissioning in 2020 January, Spitzer continued observations of SN sites in the framework of the SPIRITS project (see the latest summary of its results in Jencson et al. 2019), or by following nearby, high-priority targets such as the dust-forming Type II-P SN 2017eaw (Tinyanont et al. 2019a; Szalai et al. 2019b). A targeted SN survey by our group, LASTCHANCE, was also carried out between 2018 August and 2020 January, aiming to collect further mid-IR photometric data points on a number of SNe in order to examine the long-term evolution of different types of stellar explosions.

In this paper, we present the results of our survey, focusing primarily on interacting SNe, which constitute the vast majority of the targets we observed. In Section 2, we describe the steps of the data collection and photometry of Spitzer/IRAC data. We present our results in Section 3, and discuss our conclusions in Section 4.

2. Observations and Data Analysis

2.1. Targets of Our Study

During our Spitzer/LASTCHANCE program (PID 14098; PI O. D. Fox), we observed 31 targets that met one of the following criteria: (i) high-profile, well-understood interacting and/or dust-forming SNe that were previously detected by Spitzer/IRAC and required another epoch to monitor their mid-IR evolution (based on Szalai et al. 2019a, and references therein), or (ii) young ($\lesssim$1 yr) and relatively nearby ($\lesssim$70 Mpc) SNe with known dense CSM (from optical spectra) or with the potential for dust formation in their ejecta (Type II-P SNe).

Our observations were designed to attain a signal-to-noise ratio (S/N) of 100 for a medium background according to the Spitzer/IRAC Sensitivity Performance Estimation Tool (SENS-PET). We aimed for this S/N so that any photometric uncertainties would be dominated by systematic effects associated with the background (host-galaxy) subtraction rather than insufficient integration time. This S/N also provides a buffer for detecting SNe that may have faded more quickly than predicted. Our observations used the medium-scale cycling dither pattern to provide good redundancy and capability for self-calibration.

Basic data on the SNe and their hosts—collected via the Open Supernova Catalog[15] (Guillochon et al. 2017), Simbad database[16] (Wenger et al. 2000), and NASA/IPAC Extragalactic Database[17]—are shown in Table 1. All of our LASTCHANCE targets were observed at one epoch—except SNe 2004dk and 2018fhw (two epochs) and 2017hcc (three epochs)—in both the 3.6 and 4.5 μm channels. We also checked the Spitzer Heritage Archive (SHA)[18] for pre-explosion Spitzer/IRAC images of the SN sites, to be used as templates (see next section).

2.2. Object Identification and Photometry

We collected and analyzed IRAC post-basic calibrated data (PBCD). The scale of these images is $0\farcs6$ pixel^{-1}. Photometric analysis was carried out using the `phot` task of IRAF.[19] For

[15] https://sne.space
[16] http://simbad.u-strasbg.fr/simbad/
[17] http://ned.ipac.caltech.edu/
[18] http://sha.ipac.caltech.edu.
[19] IRAF is distributed by the National Optical Astronomy Observatories, which are operated by the Association of Universities for Research in Astronomy, Inc., under cooperative agreement with the National Science Foundation (NSF).

Table 1
Basic Data on the Studied SNe

Object	SN Type	Discovery (MJD)	Host Galaxy	α (J2000)	δ (J2000)	d (Mpc)	$E(B-V)$[a] (mag)	References
SN 1995N	IIn	49842	MCG-02-38-17	14:49:28.31	−10:10:14.0	24.0 ± 4.0	0.10	1
SN 2001em	Ib/c	52172	UGC 11794	21:42:23.60	+12:29:50.3	71.6 ± 0.7	0.10	2, 3
SN 2003gk	Ib	52821	NGC 7460	23:01:42.99	+02:16:08.7	41.2 ± 6.0	0.08	4
SN 2004dk	Ib	53218	NGC 6118	16:21:48.93	−02:16:17.3	24.0 ± 2.0	0.14	5
SN 2005ip	IIn	53679	NGC 2906	09:32:06.42	+8:26:44.4	30.0 ± 7.2	0.04	6
SN 2006jd	IIn	54020	UGC 4179	08:02:07.43	+00:48:31.5	77.0 ± 5.0	0.05	7
SN 2009ip	IIn/imp.	56193	NGC 7259	22:23:08.30	−28:56:52.0	20.5 ± 2.0	0.02	7
SN 2010jl	IIn	55503	UGC 5189A	09:42:53.33	+09:29:41.8	48.9 ± 3.4	0.02	8
SN 2010mc	IIn	55428	anon.	17:21:30.68	+48:07:47.4	159.0[b]	0.02	9, 10
SN 2011ft	Ib	55803	UGC 11021	17:52:42.98	+29:04:10.6	101.0 ± 3.0	0.06	11, 12
PTF11iqb	IIn	55765	NGC 151	00:34:04.84	−09:42:17.9	42.3 ± 11.5	0.03	13
PTF11kx	Ia-CSM	55579	anon.	08:09:12.87	+46:18:48.8	200.0[b]	0.04	14
SN 2012aw	II-P	56002	NGC 3351	10:43:53.73	+11:40:17.6	8.8 ± 1.1	0.02	15
SN 2012ca	Ia-CSM	56042	ESO 336-09	18:41:07.25	−41:47:38.4	80.0 ± 6.0[b]	0.07	16, 17
SN 2013L	IIn	56314	ESO 216-G39	11:45:29.55	−50:35:53.1	75.0 ± 5.0[b]	0.11	18
SN 2013cj	IIn	56421	UGC 10685	17:04:52.95	+12:55:10.4	135.0 ± 10.0[b]	0.09	19
SN 2013ej	II-P/L	56497	NGC 628	01:36:48.16	+15:45:31.0	9.5 ± 0.6	0.06	20
SN Hunt248	IIn/imp.	56798	NGC 5806	14:59:59.47	+01:54:26.6	20.0 ± 3.0[b]	0.04	21
ASSASN-14dc	IIn	56832	PGC 2035709	02:18:37.82	+33:37:01.7	183.0 ± 20.0[b]	0.06	22
SN 2015da	IIn	57031	NGC 5337	13:52:24.11	+39:41:28.6	30.0 ± 10.0[b]	0.02	23
AT2016jbu	IIn/imp.	57723	NGC 2442	07:36:25.96	−69:32:55.3	21.0 ± 1.5	0.2	24, 25
SN 2017aym	II-P	57766	NGC 5690	14:37:41.78	+02:17:08.4	18.6 ± 3.0	0.04	3, 26
SN 2017eaw	II-P	57887	NGC 6946	20:34:44.24	+60:11:36.0	6.9 ± 0.6	0.4	27
SN 2017ejx	II-P	57903	NGC 2993	09:45:48.61	−14:22:05.7	30.5 ± 5.0[b]	0.05	28, 29
SN 2017gas	IIn	57975	anon.	20:17:11.32	+58:12:08.0	42.0 ± 5.0[b]	0.33	30
SN 2017hcc	IIn	58028	anon.	00:03:50.58	−11:28:28.8	72.0 ± 6.0[b]	0.03	31
SN 2017ivu	II-P	58098	NGC 5962	15:36:32.70	+16:36:19.4	30.7 ± 4.0	0.05	3, 32
SN 2017jfs	IIn/LRN	58113	NGC 4470	12:29:37.79	+07:49:35.2	33.0 ± 5.0	0.02	33, 34
SN 2018gj	II	58132	NGC 6217	16:32:02.30	+78:12:40.9	24.0 ± 3.0	0.04[b]	35
SN 2018zd	IIn	58179	NGC 2146	06:18:03.18	+78:22:00.9	15.2 ± 4.0	0.08	36, 37
SN 2018acj	II-P	58185	UGC 8733	13:48:40.63	+43:25:04.7	32.1 ± 5.0	0.02	3, 38
SN 2018fhw	Ia-CSM(?)	58351	anon.	04:18:06.20	−63:36:56.4	74.2 ± 4.0	0.03	39

Notes. References: [1]Van Dyk (2013); [2]Papenkova et al. (2001); [3]Sorce et al. (2014); [4]Theureau et al. (2007); [5]Springob et al. (2009); [6]Fox et al. (2010); [7]Fox et al. (2011); [8]Fox et al. (2013); [9]Howell & Murray (2012); [10]Ofek (2012); [11]Balanutsa & Lipunov (2011); [12]Prieto (2011); [13]Parrent et al. (2011); [14]Graham et al. (2017); [15]Siviero et al. (2012); [16]Drescher et al. (2012); [17]Inserra et al. (2012); [18]Tinyanont et al. (2016); [19]Jin et al. (2013); [20]Mauerhan et al. (2017); [21]Mauerhan et al. (2015); [22]Holoien et al. (2014); [23]Zhang & Wang (2015); [24]Cartier et al. (2017); [25]Fraser et al. (2017); [26]Taddia et al. (2017); [27]Szalai et al. (2019b); [28]Brimacombe et al. (2017); [29]Kostrzewa-Rutkowska et al. (2017); [30]Balam (2017); [31]Dong et al. (2017); [32]Itagaki (2017); [33]Berton et al. (2018); [34]Pastorello et al. (2019a); [35]Kilpatrick et al. (2018); [36]Zhang et al. (2018); [37]Gao & Solomon (2004); [38]Lin et al. (2018); [39]Vallely et al. (2019).
[a] Galactic extinction.
[b] Distance calculated from redshift.

isolated sources, we implemented aperture photometry on the PBCD frames using the `phot` task as a first step. We generally used an aperture radius of 2″ and a background annulus from 2″ to 6″ (2−2–6 configuration), and applied aperture corrections of 1.213, 1.234, 1.379, and 1.584 for the four IRAC channels (3.6, 4.5, 5.8, and 8.0 μm, respectively) as given in the IRAC Data Handbook; however, for a few bright sources extending to more pixels, we used the 3−3−7 configuration (aperture corrections: 1.124, 1.127, 1.143, and 1.234, respectively).

Identifying a point source within a host galaxy, where compact H II regions and star clusters may also appear as pointlike sources in the images, can be difficult, especially if the target is faint or is superposed on a complex background. Therefore, when available, we also performed aperture photometry on template images (i.e., pre-explosion images, or very late-time images in which no point source appears at the position of the SN) and subtracted these on-site flux values from the SN fluxes. We call this technique "template-based background subtraction," or simply "background subtraction" hereafter.

Not all targets have templates. In these cases, the local background was estimated by measuring the nearby flux with apertures placed adjacent to the SN site in locations that qualitatively appear similar to the background underlying the SN (as was applied, e.g., by Fox et al. 2011). More complex modeling of the local background is beyond the scope of this paper.

In both background-subtracted and unsubtracted cases, we defined the source as a positive detection if (i) it showed epoch-to-epoch flux changes, and (ii) its flux was *above* the local background by at least 5 μJy and 15 μJy at 3.6 and 4.5 μm, respectively (according to point-source sensitivities in Table 2.10 of the IRAC Instrument Handbook[20]).

Following these steps, we find that 19 of 31 targets are detected (one object, SN 1995N, only at 4.5 μm). In three other cases (SNe 2011ft, 2017gas, and 2018fhw), there is a point

[20] https://irsa.ipac.caltech.edu/data/SPITZER/docs/irac/iracinstrumenthandbook/

source close to the coordinates of the SN; however, given the lack of template images, they cannot be confirmed. SN 2017gas is very close to the core, while SN 2011ft is a distant object that cannot be distinguished from its host (note that this latter site was also captured ∼6 yr earlier with Spitzer, but only at 3.6 μm, and there are no significant flux changes compared to this previously published value; see Szalai et al. 2019a). We discuss the case of SN 2018fhw later.

In the cases of the remaining nine targets, no point sources are detected at the position of the SN. Instead, some of these nondetections provided us with template images, which allowed us to carry out background subtraction on earlier archive data on these particular targets. In the cases of PTF11kx, SNHunt248, ASASSN-14dc, SN 2009ip, and SN 2012ca, background subtractions do not change the previously published flux values (see Szalai et al. 2019a, and references therein) beyond photometric uncertainties. Instead, the change in measured flux is more significant in the case of SN 2001em (221 ± 41 and 294 ± 36 μJy at 3.6 and 4.5 μm, respectively, versus 303 ± 41 and 349 ± 37 μJy given in Szalai et al. 2019a) located in a distant, nearly edge-on galaxy. We included updated fluxes and correponding absolute magnitudes of SN 2001em in Table 2.

Moreover, during the review of archival Spitzer data, we identified a variable mid-IR source at the position of the Type Ib SN 2003gk. While there are no published Spitzer data for this object (we missed it during our overview in Szalai et al. 2019a), we added it to our sample and analyzed it in the same way as the other targets (discussed in more detail below). In the case of the Type II-P SN 2017eaw, we also present here the previously unpublished photometry of late-time archival data.

In summary, we studied 32 objects during this program: 13 SNe IIn (11 positive detections, 1 unconfirmed detection, 1 nondetection), 7 SNe II-P (4 positive detections, 3 nondetections), 1 unclassified SN II (positive detection), 4 SNe Ib/c (2 positive detections, 1 unconfirmed detection, 1 nondetection), 3 SNe Ia-CSM (1 unconfirmed detection, 2 nondetections), and 4 intermediate-luminosity transients (2 positive detections, 2 nondetections). These detection rates—taking into account epochs and distances—are basically in agreement with the expectations based on earlier results (Tinyanont et al. 2016; Szalai et al. 2019a); see details later. For 12 of our targets, no Spitzer data have been published before (Type IIn PTF11iqb, ASASSN-14dc, SN 2015da, and SN 2017hcc; Type II-P SNe 2017aym, 2017ivu, 2018gj, 2018acj; SNe Ib 2003gk and 2004dk; and intermediate-luminosity transients AT2016jbu and SN 2017jfs).

In Figure 1, we present examples of new positive detections (SNe 2004dk, 2017hcc, and 2017jfs). Mid-IR fluxes and cases of nondetections are listed in Table 2. We also identify SNe where background subtraction was not possible. We note that in all these cases, the measured fluxes should be interpreted as upper limits given the complex underlying backgrounds. Flux uncertainties are generally based on photon statistics provided by `phot`; however, where background-subtraction photometry was carried out, an increase in the noise level by $\sqrt{2}$ is also taken into account.

3. Results

Szalai et al. (2019a) first published the comprehensive mid-IR light curves (LCs) of SNe based on their complete data sets available at that time. In this work, we present new Spitzer data points for several SNe. Furthermore, we compare the long-term mid-IR evolution of different types of interacting SNe. We also present our findings on connections between mid-IR behavior and level of circumstellar interaction observed in other wavelength regions.

3.1. Long-term Mid-IR LCs

In Figure 2, we present 4.5 μm LCs of all SNe in our current sample and of some further well-known interacting SNe, along with their corresponding Spitzer archival data previously published by Szalai et al. (2019a, and references therein).

The newest data originate primarily in this work, although some additional data from Jencson et al. (2019) and Tinyanont et al. (2019b) are also included (see details in Sections 3.1.3 and 3.1.5). We also present the 4.5 μm LCs of our SNe in Figure 3 for four subgroups: SNe IIn, SNe Ia-CSM, SNe Ib/Ic, and intermediate-luminosity transients.

3.1.1. Type IIn SNe

In Figure 3, existing mid-IR LCs of all SNe IIn are presented; LASTCHANCE targets and some further well-sampled objects are highlighted. SNe IIn form a bright but somewhat heterogeneous group in the mid-IR. Some extremely luminous objects reach a maximum brightness of ∼−22 mag at 4.5 μm, such as SN 2010jl (Andrews et al. 2011a; Fransson et al. 2014; Szalai et al. 2019a), SN 2006jd (Fox et al. 2010; Stritzinger et al. 2012; Szalai et al. 2019a), SN 2007rt (Fox et al. 2011, 2013; Szalai et al. 2019a), and SN 2013cj (Szalai et al. 2019a). Other SNe IIn are much fainter in the mid-IR (i.e., SN PTF11iqb). Some objects even fall into the brightness gap that seems to exist between the previously mentioned objects (i.e., SN 2010mc).

Most SNe IIn are still bright in our most recent Spitzer observations, in some cases ∼4500–5000 days (12–13 yr!) after explosion. The one SN IIn exception to this is ASASSN-14dc, which is not detectable at ∼1600 days (but it is a very distant object, $d \approx 180$ Mpc). We note that SN 1995N is still barely detectable in the 4.5 μm image obtained during our LASTCHANCE survey at an age of ∼8600 days (making it the latest-observed SN IIn in the mid-IR).

The decline rates of the mid-IR LCs of SNe IIn vary from ∼0.4 mag $(1000 \text{ days})^{-1}$ up to ∼3.0 mag $(1000 \text{ days})^{-1}$; see Table 3. If we compare these values with the mid-IR LC evolution of the objects (Figures 2 and 3), we can see that the brightest ones (SNe 2007rt, 2010jl, and 2013cj) exhibit a faster decline after ∼1000 days. In the case of SN 2010jl, comprehensive multiwavelength studies and detailed analyses of ongoing dust formation exist (e.g., Andrews et al. 2011a; Gall et al. 2014; Fransson et al. 2014; Sarangi et al. 2018; Bevan et al. 2020); unfortunately, there are no similar data sets in the cases of SN 2007rt and SN 2013cj. Another group of SNe IIn (SNe 2005ip, 2006jd, and 2013L) seem to be a bit fainter during the first ∼2000 days (note, however, that in the first two cases there are no mid-IR data before ∼950 days and ∼1150 days, respectively), but decline more slowly thereafter. In these SNe, the most probable scenario is a large, pre-existing dust shell that is continuously heated by energetic photons generated by ongoing CSM interaction (see, e.g., Fox et al. 2010, 2011, 2020; Stritzinger et al. 2012; Andrews et al. 2017; Taddia et al. 2020). Based on this picture, the decline rates of these SNe may hint that the level of CSM interaction

Table 2
Previously Unreported Mid-IR (Spitzer) Detections and Nondetections (Fluxes and Vega Magnitudes) of Interacting SNe

Object	Type	Date (MJD)	Epoch[a] (days)	$F_{\nu,[3.6]}$ (μJy)	$F_{\nu,[4.5]}$ (μJy)	Absolute Mag. 3.6 μm	Absolute Mag. 4.5 μm
SN 1995N	*IIn*	58,419	8577	<5	13(5)	−12.5<	−14.06(0.62)
SN 2001em[b]	Ib/c	53,307	1135	221(41)	294(36)	−19.02(0.20)	−19.81(0.13)
		58,541	6369	<82	<55	−17.9<	−18.0<
SN 2003gk[c]	Ib	55,939	3118	⋯	2438(83)	⋯	−20.45(0.31)
		56,160	3339	⋯	2062(75)	⋯	−20.27(0.31)
		56,536	3715	⋯	1510(65)	⋯	−19.93(0.32)
		56,699	3878	⋯	1336(61)	⋯	−19.79(0.32)
		56,912	4091	⋯	1123(56)	⋯	−19.61(0.32)
		57,819	4998	⋯	651(43)	⋯	−19.02(0.33)
		58,031	5210	⋯	592(42)	⋯	−18.91(0.33)
		58,204	5383	⋯	556(39)	⋯	−18.84(0.33)
SN 2004dk	*Ib*	55,115	1897	85(16)	93(16)	−15.62(0.28)	−16.19(0.26)
		58,457	5239	141(20)	201(24)	−16.17(0.24)	−17.03(0.22)
		58,852	5634	130(20)	183(23)	−16.08(0.24)	−16.93(0.22)
SN 2005ip	*IIn*	58,346	4667	677(51)	713(47)	−18.34(0.52)	−18.88(0.52)
SN 2006jd	*IIn*	58,345	4325	82(15)	106(17)	−18.11(0.24)	−18.86(0.22)
SN 2009ip	*IIn/imp.*	58,529	2336	<3	<5	−11.6<	−12.7<
SN 2010jl	IIn	58,372	2869	300(42)	611(47)	−18.52(0.21)	−19.78(0.17)
SN 2010mc	*IIn*	58,411	2983	33(9)	37(10)	−18.72(0.34)	−19.31(0.32)
PTF11iqb	*IIn*	57,089	1324	120(20)	143(21)	−17.21(0.61)	−17.89(0.61)
		58,405	2640	64(15)	51(13)	−16.54(0.64)	−16.76(0.65)
PTF11kx	*Ia-CSM*	58,516	2866	<5	<15	−17.1<	−18.8<
SN 2012aw	II-P	58,366	2364	<5	<15	− 10.4 <	− 12.0 <
SN 2013L	*IIn*	58,405	2091	289(28)	506(37)	−19.42(0.18)	−20.50(0.16)
SN 2012ca	*Ia-CSM*	58,490	2448	<5	<15	−15.2<	−16.8<
SN 2013cj	*IIn*	58,457	2036	119(18)	214(24)	−19.73(0.23)	−20.84(0.20)
SN 2013ej	II-P/L	58,427	1930	<5	<15	− 10.5 <	− 12.2 <
SNHunt248	IIn/imp.	58,419	1621	<5	<15	− 12.1 <	− 13.8 <
ASSASN-14dc[d]	IIn	57,323	491	176(37)	217(35)	−20.81(0.33)	−21.51(0.29)
		58,466	1634	<320	<220	−20.7<	−20.7<
SN 2015da	IIn	58,404	1373	1603(69)	2155(79)	−19.28(0.72)	−20.08(0.72)
AT2016jbu	IIn/imp.	58,352	629	67(16)	90(18)	−15.07(0.31)	−15.87(0.27)
SN 2017aym	II-P	58,415	649	265(79)	303(59)	−16.29(0.47)	−16.91(0.41)
SN 2017eaw	II-P	58,404	517	124(18)	314(30)	−13.07(0.25)	−14.76(0.21)
		58,488[e]	601	78(15)	149(20)	−12.83(0.25)	−14.00(0.22)
		58,515[f]	628	79(15)	128(20)	−12.85(0.28)	−13.83(0.22)
		58,529[e]	642	75(16)	132(19)	−12.79(0.28)	−13.87(0.24)
		58,567[e]	680	58(14)	83(18)	−12.51(0.28)	−13.37(0.24)
		58,607[e]	720	88(16)	121(19)	−12.96(0.27)	−13.78(0.25)
		58,795[e]	908	49(12)	57(13)	−12.34(0.32)	−12.97(0.31)
SN 2017ejx	II-P/L	58,373	470	<5	<15	− 13.1 <	− 14.7 <
SN 2017hcc	*IIn*	58,420	392	1818(70)	1813(71)	−21.32(0.18)	−21.79(0.18)
		58,593	565	1533(64)	1703(69)	−21.13(0.18)	−21.72(0.18)
		58,795	767	1097(55)	1354(62)	−20.77(0.18)	−21.47(0.18)
SN 2017ivu	II-P	58,416	318	41(15)	68(20)	−15.35(0.37)	−16.38(0.31)
SN 2017jfs	IIn/LRN	58,402	289	100(44)	63(31)	−16.48(0.58)	−16.46(0.63)
SN 2018gj	II	58,484	352	17(7)	83(15)	−13.91(0.50)	−16.06(0.33)
SN 2018zd	IIn	58,507	328	40(13)	73(15)	−13.80(0.68)	−14.93(0.62)
SN 2018acj	II-P	58,391	206	15(6)	27(8)	−14.41(0.57)	−15.50(0.48)

Notes. We show here all new measurements from our LASTCHANCE program, together with unpublished archive data on SNe 2003gk and 2017eaw. Data shown in italics denote cases where template-based background subtraction cannot be applied—given the lack of either pre-explosion or late-time images (in all these cases, measured fluxes can be considered only as upper limits).

[a] Days since discovery.

[b] Corrected fluxes/magnitudes determined after background subtraction based on recently obtained Spitzer images in which the target is not detectable; data paper contains the original fluxes: Szalai et al. (2019a).

[c] Target detection (SN 2003gk) in archive images: PIDs 90007 and 13012 (PI J. D. Kirkpatrick).

[d] Positive detections in archive images after background subtraction based on recently obtained Spitzer images in which the target is not detectable: ASASSN-14dc—PID 11053 (PI O. Fox).

[e] Archive data (PID 14089, PI M. Kasliwal).

[f] Archive data (PID 13239, PI K. Krafton).

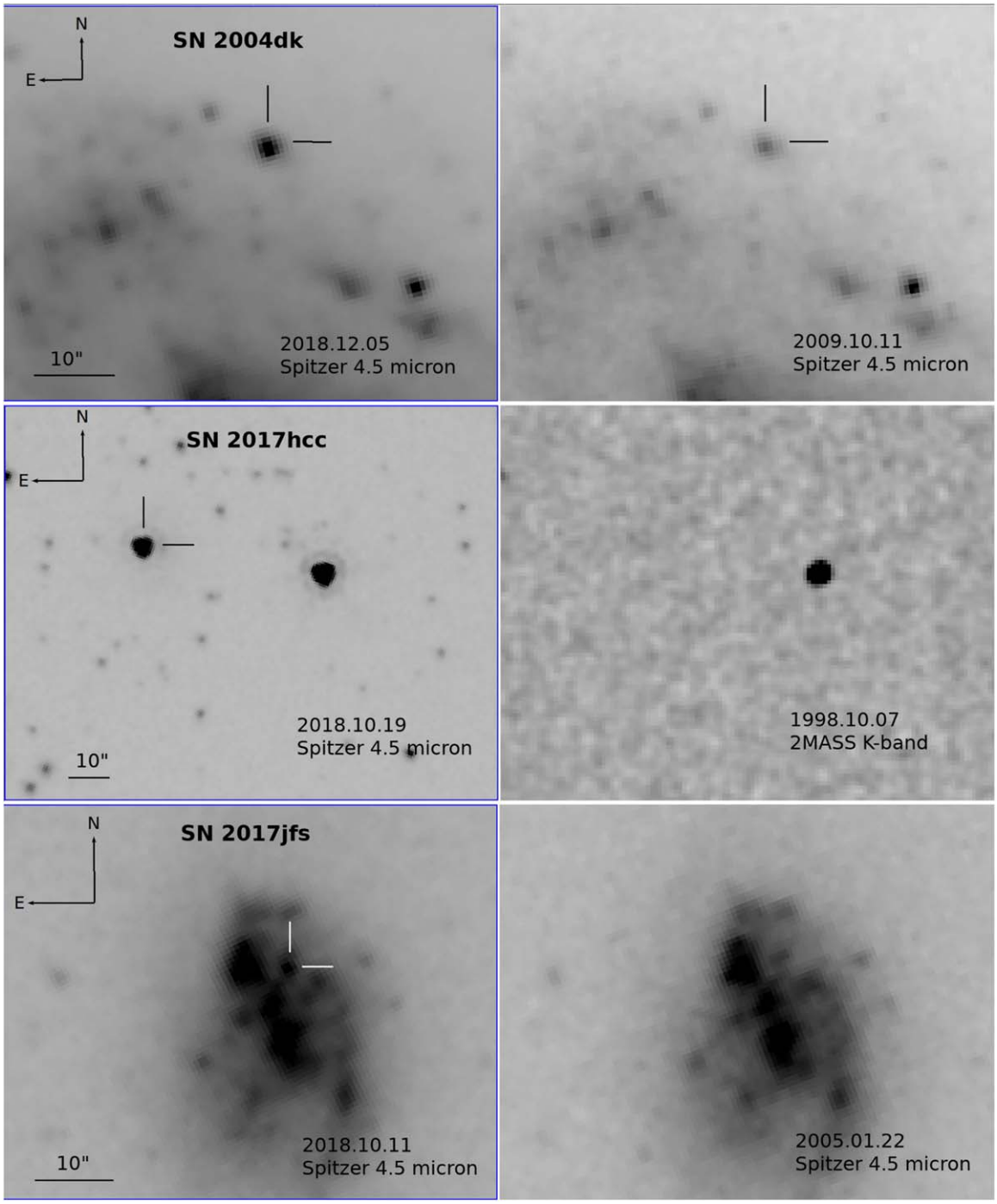

Figure 1. Examples of new positive detections in Spitzer/IRAC 4.5 μm images. Top: SN 2004dk (Type Ib, post-explosion images after (left) and before (right) mid-IR rebrightening). Middle: SN 2017hcc (Type IIn, post-explosion image (left) and archival Two Micron All Sky Survey K_s-band image (right)). Bottom: SN 2017jfs (luminous red nova, post-explosion (left) and pre-explosion (right) Spitzer images).

continuously decreases in the last years (except in the case of SN 2010mc, which seems to be in a very long "plateau" phase even at ~3000 days).

SN 2017hcc stands out among our LASTCHANCE sample because of its unusually high degree of polarization (Mauerhan et al. 2017; Kumar et al. 2019) and the post-shock dust formation assumed from the analysis of its strongly blueshifted line profiles (Smith & Andrews 2020). The SN was observed at three epochs (392, 565, and 767 days) by Spitzer. While at the earliest epoch, SN 2017hcc resembles SN 2010jl in the mid-IR, its fluxes do not increase after that but start to slowly decrease, similar to the LC of (for example) SN 2005ip.

3.1.2. Type Ia-CSM SNe

SNe Ia-CSM are comparably luminous to SNe IIn. This subclass is thought to arise from thermonuclear explosions surrounded by dense, H-rich shells of ambient CSM (producing SN IIn-like emission features in their late-time spectra; see, e.g., Silverman et al. 2013; Fox et al. 2015; Inserra et al. 2016).

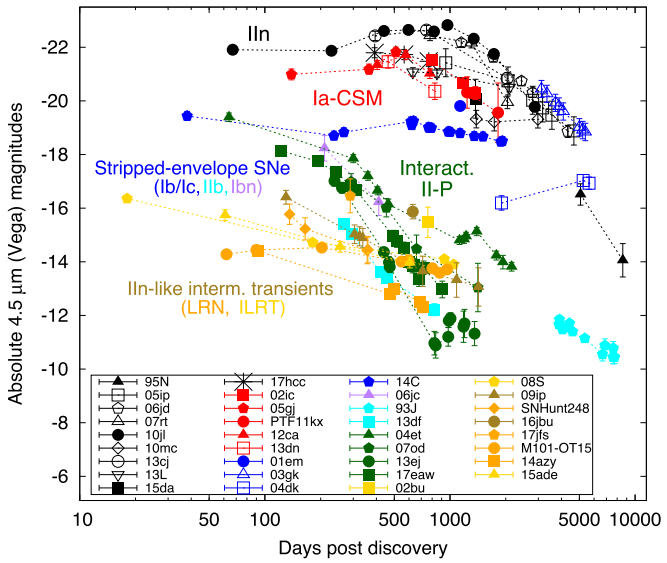

Figure 2. Spitzer 4.5 μm evolution of various types of interacting SNe. Sources of data are Szalai et al. (2019a) and references therein, Tinyanont et al. (2019a), Jencson et al. (2019), and this work, as also highlighted in the text and in Table 2. Filled symbols denote SNe whose absolute magnitudes were determined with background subtraction (using either pre-explosion or very late-time reference images), while empty symbols, crosses, and asterisks denote objects where no background subtraction was possible.

Few SNe Ia-CSM have been observed by Spitzer; Figures 2 and 4 show all of them. Analysis of this small sample suggests that this subclass, particularly in the mid-IR, is more homogeneous than SNe IIn (Graham et al. 2017; Szalai et al. 2019a). Only SN 2012ca is observed around the mid-IR "peak," reaching an absolute magnitude of almost -22 at 4.5 μm around 600 days after explosion, but the other objects in this subclass do seem to follow a qualitatively similar evolution. Apart from SN 2013dn, we also do not detect any of the SNe Ia-CSM between 1500 days and 3500 days after explosion.

We also discuss two nondetections of SN 2018fhw (ASASSN-18tb), the only new thermonuclear SN Ia in our sample. This object has unique optical properties that show some similarities but also striking differences to other SNe Ia-CSM (Kollmeier et al. 2019; Vallely et al. 2019). We observed the site of SN 2018fhw at two epochs ($\sim$250 days and $\sim$450 days after explosion). While there is a pointlike source in all of the images, its position does not exactly match that of the SN (its center is $\sim 2''$ from the position given by Vallely et al. (2019), see Figure 5; moreover, it does not show flux changes (within the uncertainties) between the two epochs in any channels. Given the lack of pre-explosion template images, we conclude for the moment that the source is not detected in our data. If we do calculate the absolute magnitudes of the detected mid-IR source, we obtain ~ -17 mag in both IRAC channels, which is a much lower value than that of other studied SNe Ia-CSM at these epochs.

3.1.3. Stripped-envelope SNe

Given their lack of significant CSM, stripped-envelope (SE) SNe (i.e., SNe Ibc) usually have uneventful mid-IR histories, producing a relatively quick fading and a disappearance after several hundred days. Some SNe IIb are detected in the mid-IR up to almost 1000 days, which may be the sign of some (moderate) late-time CSM interaction; see Szalai et al. (2019a) and references therein. Note that the Type IIb SN 1993J stands out owing to its proximity (3.5 Mpc) and uncomplicated local background, detectable in IRAC imaging up to almost 8000 d (Tinyanont et al. 2016).

There is now more than one known "normal" SE SN that has been observed to transform into a strongly interacting, SN IIn-like object at later times. The most well-studied event is the nearby ($d \approx 13$ Mpc) Type Ib SN 2014C (Milisavljevic et al. 2015; Margutti et al. 2017). This object is also among the most well-sampled SNe with Spitzer, since its host galaxy is NGC 7331, one of the target galaxies for the SPIRITS program (Tinyanont et al. 2016, 2019b). SN 2014C was followed out to $\sim$2000 days (until the end of the Spitzer mission). During that time, it showed a clear rebrightening at $\sim$250 days as the CSM interaction began, and a very slow fading thereafter (it is still a bright source in the latest images).

Another unique SN Ib/c that shows CSM interaction is SN 2001em. It had only one previous epoch of Spitzer data in 2004. Increasing CSM interaction was detected at optical, X-ray, and radio wavelengths at that point (see, e.g., Pooley & Lewin 2004; Soderberg et al. 2004; Stockdale et al. 2004). While the object appears as a very bright source in the original imaging, our most recent nondetection provides a useful template (at 3.6 μm and 4.5 μm) that results in improved and updated mid-IR fluxes of SN 2001em at $\sim$1100 days (which are $\sim$20%–25% lower than those published by Szalai et al. 2019a). Figure 3 shows that SN 2001em was even more luminous in the mid-IR than SN 2014C, almost as bright as most SNe IIn or SNe Ia-CSM.

While it was not possible to carry out the same process on 5.8 and 8.0 μm data, SN 2001em appears as a very bright point source in those images, too. We concur that the previous conclusion of Szalai et al. (2019a) still holds true, namely that (i) a two-component mid-IR spectral energy distribution (SED) in 2004 indicates the presence of multiple pre-explosion dust shells, and (ii) a few times 10^{16} cm for the shell radius and a total circumstellar dust mass of a few times 0.01 $M_{\odot}$, both of which (assuming a dust-to-gas mass ratio of 0.01) are in agreement with the results of Chugai & Chevalier (2006) and Chandra et al. (2020).

We also highlight the initially "normal" Type Ib/c SN 2004dk, which has started to show unexpected, strong signs of CSM interaction in the form of enhanced Hα and X-ray emission more than a decade after its explosion (Mauerhan et al. 2018a; Pooley et al. 2019). (Note that in their earlier study, Wellons et al. 2012, already found some abrupt late-time radio variability indicating unusual circumstellar environment.) Although sampling is sparse, the mid-IR properties of SN 2004dk are consistent with these findings, showing a $\sim$1 mag increase between $\sim$2000 days and 5000 days, subsequently slowly fading by the third epoch. This is the latest-time mid-IR brightening observed in our sample. Only SN 1987A has shown an increase in mid-IR emission at a later epoch, with continuously increasing mid-IR fluxes between $\sim$6000 days and 8500 days (Arendt et al. 2020, and references therein).

Finally, we highlight SN 2003gk. Although we do not have any recent observations, we include archival 4.5 μm Spitzer/IRAC images uncovered during the writing of this paper. SN 2003gk is well sampled at 3.6 μm in the range 3100–5400 days and shows a qualitatively similar evolution to that of the long-term monitored SNe IIn 2005ip and 2006jd. There is only

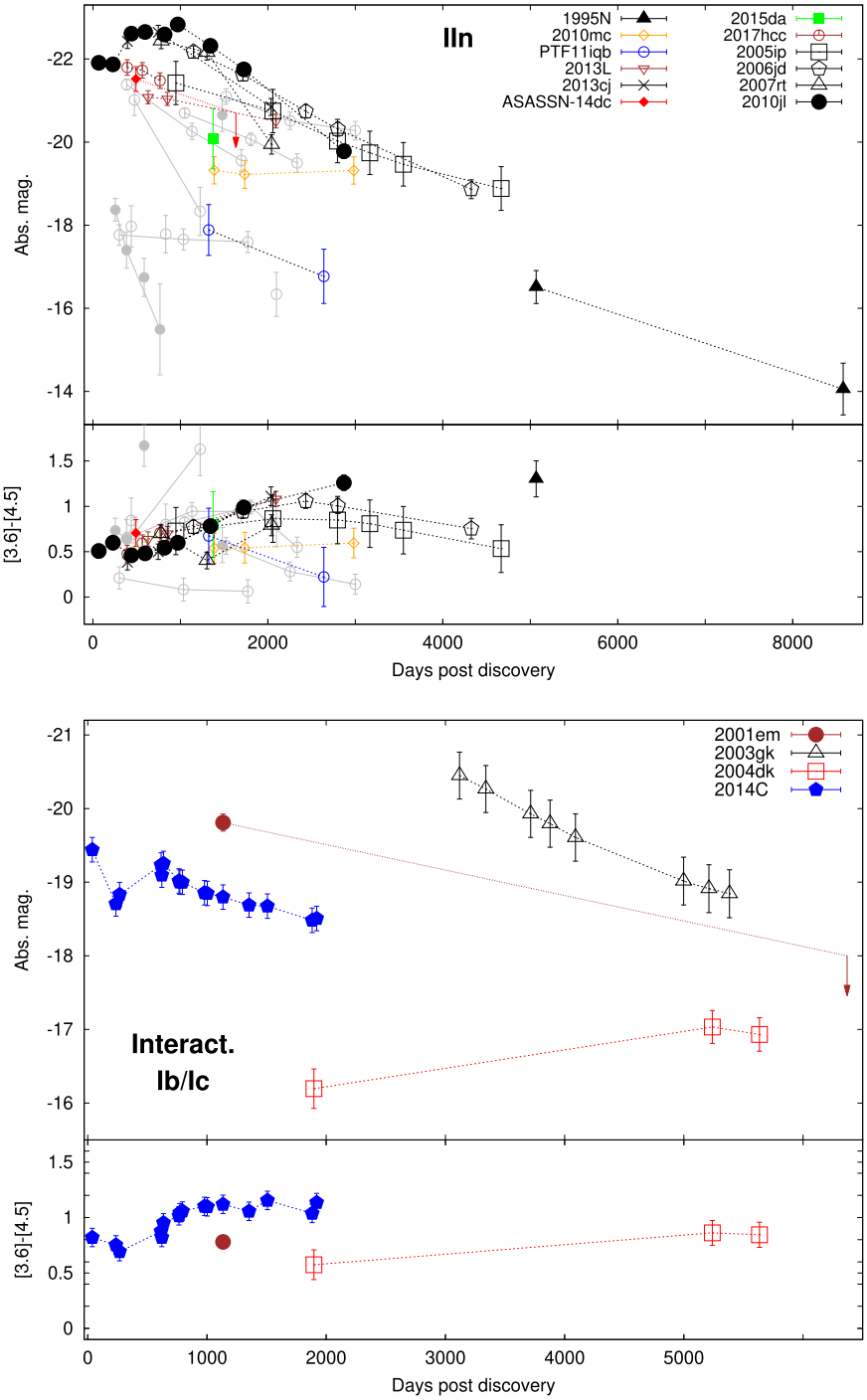

Figure 3. 4.5 μm absolute magnitudes of all SNe IIn and interacting SNe Ib/c ever observed by Spitzer (data points are the same as in Figure 2, but graphs are zoomed-in and timescales are linear), together with [3.6] – [4.5] μm color curves (all in Vega magnitudes). LASTCHANCE and some further well-sampled objects are highlighted, while all other published detections (adopted from Szalai et al. 2019a) are marked with gray symbols. Existing nondetections (upper limits) are marked with arrows. Note that no 3.6 μm measurements were obtained for the Type Ib SN 2003gk (bottom panel).

one publication on SN 2003gk in the literature (Bietenholz et al. 2014), which suggests the presence of late-time CSM interaction based on radio observations.

3.1.4. Type II-P SNe

Based on theoretical expectations (see, e.g., Kozasa et al. 2009; Gall et al. 2011), SNe II-P are likely the best candidates for (ejecta) dust formation among SNe. Some of these objects were targets of Spitzer observations in the early years of the mission. These data typically trace dust formation $\sim$1–3 yr after explosion and estimate the physical parameters of newly formed dust (e.g., Meikle et al. 2007, 2011; Sugerman et al. 2006; Kotak et al. 2009; Andrews et al. 2010; Fabbri et al. 2011; Szalai et al. 2011, 2019a; Szalai & Vinkó 2013). The results do not support either the theoretical prediction of significant ($\gg$0.001 $M_\odot$) SN dust production or the large observed dust masses in some young Galactic SN remnants and in high-redshift galaxies. This discrepancy can be partly resolved by the application of clumped dust models, or

Table 3
Decline Rates of Type IIn SNe

Object	Range of Epochs[a] (d)	$\Delta m_{3.6}$ (1000 days)$^{-1}$	$\Delta m_{4.5}$ (1000 days)$^{-1}$
SN 1995N	5067–8577	…[b]	0.7
SN 2005ip	2796–4667	0.4	0.6
SN 2006jd	2433–4525	0.8	1.0
SN 2007rt	1304–2042	3.5	3.0
SN 2010jl	969–2869	2.0	1.7
SN 2013L	850–2091	0.7	0.4
SN 2013cj	747–2036	1.8	1.4

Notes.
[a] Used to calculate decline rates at the latest phases.
[b] SN 1995N was not detectable at 3.6 μm on day 8577.

significant grain growth in the interstellar matter (see Gall et al. 2011, for a detailed review). Another possibility is that a significant amount of cold (<50 K) dust may be present in the ejecta, as can be seen via far-IR and submillimeter observations of the very nearby SN 1987A (Matsuura et al. 2011, 2015; Indebetouw et al. 2014; Wesson et al. 2015).

During our LASTCHANCE program, we collected single data points on some young SNe II-P during the assumed formation period of ejecta dust (∼200–650 days): SNe 2017aym, 2017eaw, 2017ivu, and 2018acj. Moreover, we also targeted the older SNe II-P 2012aw and 2013ej, both of which turned out to be below the detection limit. Regarding SN 2013ej (Mauerhan et al. 2017), a very late-time mid-IR rebrightening can be seen between ∼700 and 1000 days, just as in the SN II-P 2004et (Kotak et al. 2009; Fabbri et al. 2011), presumably because of dust formation in the CDS behind the reverse shock and not within the ejecta. Based on known (Tinyanont et al. 2019a; Szalai et al. 2019b) and previously unpublished Spitzer data on SN 2017eaw, it seems to produce a ghost-like similarity to SN 2004et (found in the same host galaxy!) in the mid-IR (even the small rebrightening is there at ∼700–750 days; see Figure 4). Unfortunately, Spitzer's mission ended just before the expected intense rebrightening seen in the case of SN 2004et and SN 2013ej at ∼1000–1300 days (the last Spitzer observation of SN 2017eaw was obtained in 2019 November). Nevertheless, connecting to the similarity of these three objects and the main storyline of our current paper, all of them show signs of late-time circumstellar interaction at ∼900 days observed via the emerging Hα emission-line profiles (see Weil et al. 2020).

3.1.5. Intermediate-luminosity Interacting Transients

In Figures 2 and 4, we plot both previously published and new mid-IR data points of intermediate-luminosity interacting transients. In the literature, this subclass is divided into two groups: intermediate-luminosity red transients (ILRTs) and luminous red novae (LRNe). ILRTs are typically described as explosions of deeply dust-enshrouded stars (see, e.g., Prieto et al. 2008; Bond et al. 2009; Kochanek 2011; Jencson et al. 2019). Included in our sample are SNe 2008S (Szczygieł et al. 2012b), 2002bu (Szczygieł et al. 2012a), and SPIRITS15ade (Jencson et al. 2019). LRNe are thought to be merging events of massive binaries (see, e.g., Pastorello et al. 2019b, and references therein). We included data for SN Hunt248 (Mauerhan et al. 2018b), M101-2015OT-1 (Blagorodnova et al. 2017; Jencson et al. 2019), SPIRITS14azy (Jencson et al. 2019), as well as the previously unpublished data on SN 2017jfs.

These objects are less luminous in the mid-IR than normal SNe and show a significant heterogeneity in their luminosity: at ∼300 days and ∼600–700 days, when there are data points for most of these SNe, brightness values spread over nearly a ∼3 mag range. Most well-sampled transients of that kind fade quickly, but M101-OT2015-1 shows a plateau at ∼800–960 days. These differences likely arise from different physical and/or geometric properties of the ambient dust content.

We also include Spitzer data on the well-studied SN 2009ip. Our most recent observation is a nondetection, allowing for template-based background subtraction. Our new photometry is within the original uncertainties (Fraser et al. 2015; Szalai et al. 2019a). It is worth noting that while SN 2009ip reached an optical (*R*-band) peak brightness similar to that of normal SNe IIn (∼−18 mag; see, e.g., Margutti et al. 2014) during its outburst in 2012, it is an order of magnitudes fainter in the mid-IR than either Type IIn or other "normal" interacting SNe. Based on the detailed analyses of Margutti et al. (2014), Fraser et al. (2015), and others, the quick optical fading of SN 2009ip implies that it was a low-energy explosion, while results of spectropolarimetric studies can be explained best with the presence of an inclined disk-like CSM (Reilly et al. 2017). These two effects together can explain the low, continuously decreasing mid-IR luminosity.

Finally, we highlight the single data point for AT2016jbu, which showed a spectral evolution similar to that of SN 2009ip (Fraser et al. 2017; Brennan et al. 2021a, 2021b). Its mid-IR brightness, however, is more similar to that of the ILRT-type SN 2002bu than of SN 2009ip at the epoch of our Spitzer observation. This case also suggests that the mid-IR properties of intermediate-luminosity interacting transients and therefore their local environment cannot be distinguished clearly by spectral type alone.

3.2. Mid-IR Color Curves and Dust Temperatures

Figure 3 and 4 also show [3.6] – [4.5] μm color curves in every case when data in both channels are available. Mid-IR color evolution can be, with some limitations, a good indication of temporal changes of dust temperature. In the first few hundreds of days after explosion, when hot ($T \gtrsim 1000$ K) components of gas and dust tend to dominate the ejecta and/or its environment, the IRAC measurements probe the peak of the dust blackbody emission and provide the best constraints on the physical parameters. Such measurements have been illustrated with several SNe II-P (see, e.g., Sugerman et al. 2006; Meikle et al. 2007; Kotak et al. 2009; Andrews et al. 2010, 2011b; Szalai et al. 2011; Szalai & Vinkó 2013) and several interacting SNe (SN 2005ip—Fox et al. 2010, 2020; Stritzinger et al. 2012; SN 2006jd—Stritzinger et al. 2012; SN 2010jl—Andrews et al. 2011a; Fransson et al. 2014; Sarangi et al. 2018; Bevan et al. 2020; SN 2013L—Andrews et al. 2017; Taddia et al. 2020; SN 2014C—Tinyanont et al. 2019b; SN 2015da—Tartaglia et al. 2020).

Since most of the data presented in this paper were obtained during the Warm Spitzer mission, we are limited to the 3.6 and 4.5 μm data. Longer-wavelength data would be necessary to probe (much) colder dust, which has been observed in SN 1987A (Dwek et al. 2010; Matsuura et al. 2011; Indebetouw et al. 2014) and in young Galactic SN remnants

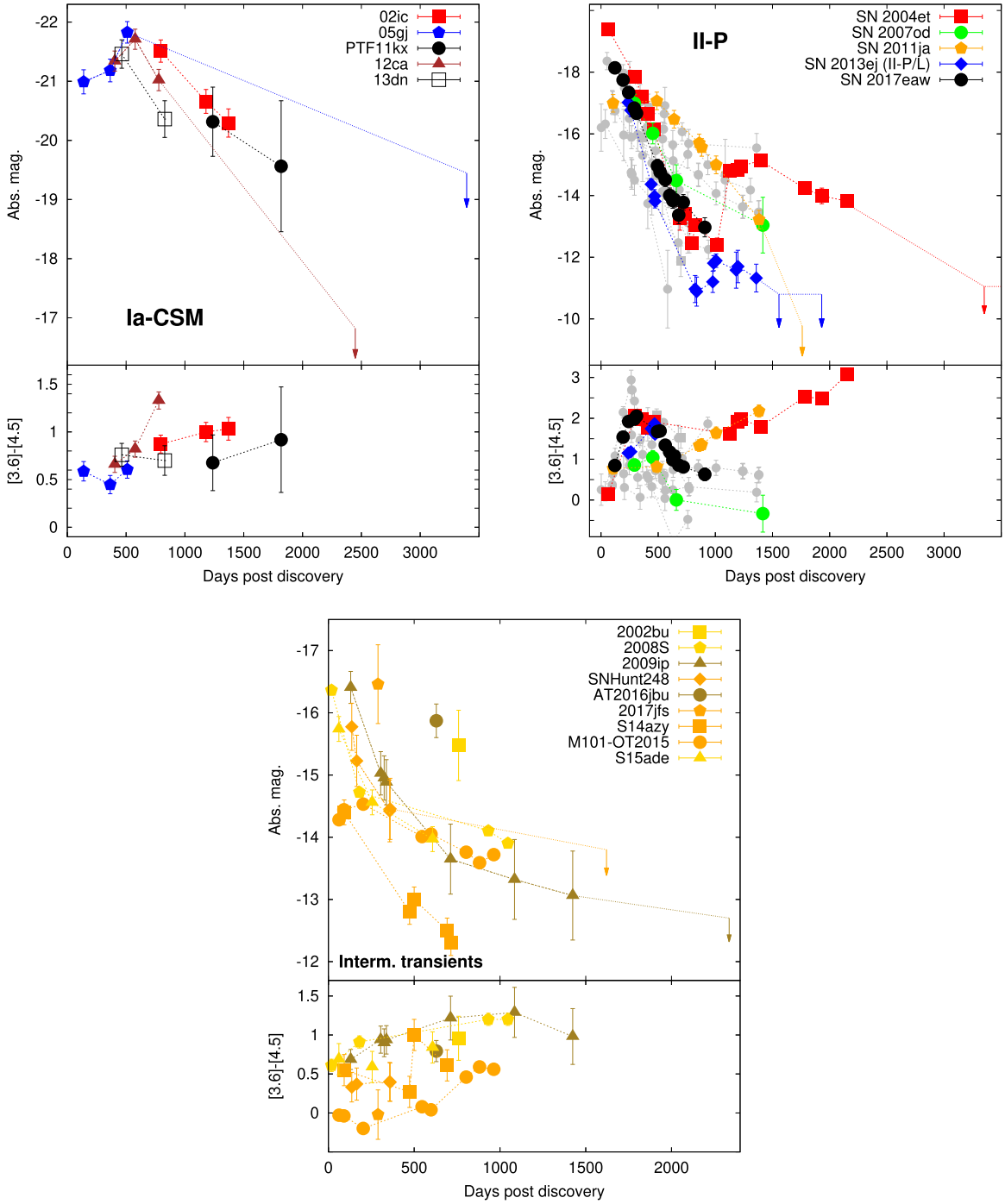

Figure 4. 4.5 μm absolute magnitudes of all SNe Ia-CSM (top left), SNe II-P (top right), and intermediate-luminosity objects (bottom) ever observed by Spitzer. Note that there are missing positive 3.6 μm detections for some of the objects. LASTCHANCE and some further well-sampled objects are highlighted, while all other published detections (adopted from Szalai et al. 2019a) are marked with gray symbols. Existing nondetections (upper limits) are marked with arrows.

(see, e.g., Williams & Temim 2017, for a review). A limited number of 5.8–24.0 μm measurements were obtained by Spitzer during its cryogenic phase on a few extragalactic SNe; from these data, the presence of cold dust can also be inferred (even within a few years after explosion, see Szalai et al. 2019a, for a review). Unfortunately, the assumed (significant) cold dust reservoirs cannot be efficiently surveyed; however, above $\sim$200 K, we will be able to get a much more detailed picture of the dust content of SNe from the expected data from the forthcoming James Webb Space Telescope (JWST).

Even with just two data points, we can derive dust temperatures and radii of the dust-containing regions via fitting blackbodies (or simple dust models) to two-point SEDs (see, e.g., Fox et al. 2011, 2013; Szalai et al. 2019a). First, it is important to determine whether any line emission contributes to the 3.6 and 4.5 μm measurements. As shown in some SNe II-P (e.g., Kotak et al. 2005; Szalai et al. 2011; Szalai & Vinkó 2013),

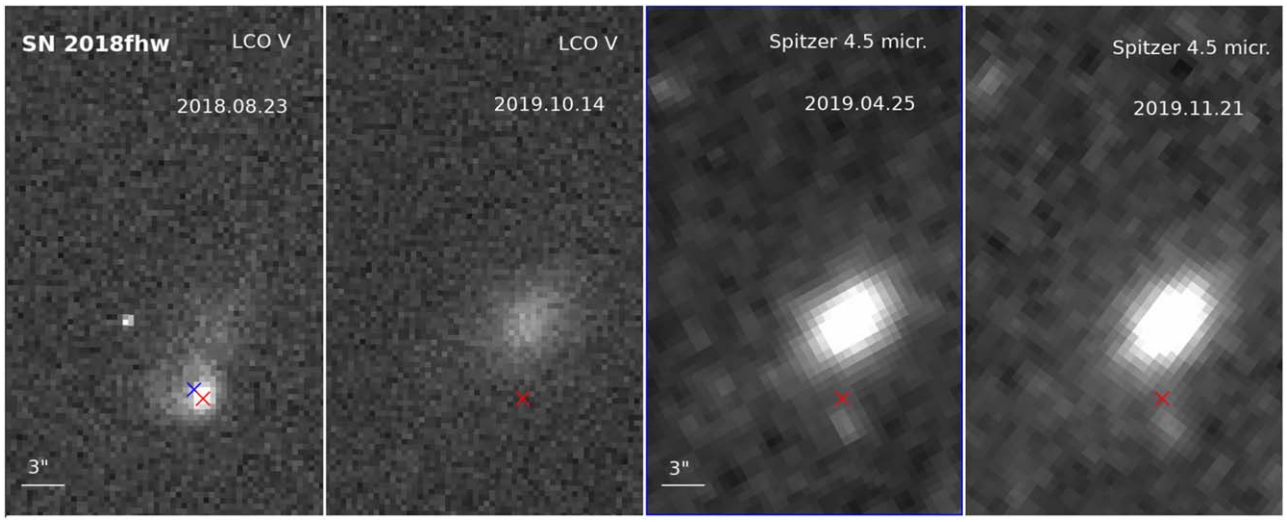

Figure 5. Optical (LCO *V*-band) and mid-IR (Spitzer 4.5 μm) images of SN 2018fhw. The blue cross (in the left panel) denotes the coordinates given by Vallely et al. (2019), while the red cross shows the photometric center of the optical (LCO) image of the source.

additional flux from the 1–0 vibrational band of CO at 4.65 μm may arise in the first ∼500 days, strongly affecting the 4.5 μm LCs and leading to values of [3.6] – [4.5] ≈ 1.5–3 mag in this period (see, e.g., SNe 2004et and 2017eaw in Figure 4).

The colors of SNe IIn have a relatively small scatter (∼0.5–0.7 mag), indicating the long-time presence of hot dust above ∼1000 K. This is in agreement with the results of Fransson et al. (2014) and Sarangi et al. (2018) on SN 2010jl and of Kokubo et al. (2019) on KISS15s. The color of SN 2010jl turns continuously redder after ∼1000 days, probably indicating the decreasing dust temperature, which is also observed in SN 2007rt and SN 2013cj (at least up to their last observed epochs). In contrast, the colors of SN 2005ip and SN 2006jd indicate nearly constant (or, at least, slowly changing) dust temperatures out to ∼4500 days, in agreement with the results of Fox et al. (2010, 2013, 2020) and Stritzinger et al. (2012). SN 2010mc seems to follow a similar trend to SN 2005ip.

SNe Ia-CSM and interacting SNe Ib/c basically show a nearly constant or slowly changing mid-IR color evolution within their observational ranges. This is in agreement with the results of previous studies (e.g., Fox & Filippenko 2013; Graham et al. 2017; Tinyanont et al. 2019b), in which the authors revealed slow evolution of dust temperatures in some of these SNe. The only exception is SN 2012ca, which shows a more intense reddening (cooling) in the first few hundred days.

The colors of interacting intermediate-luminosity transients, just like their LCs, exhibit large heterogeneity. The mid-IR color evolution of most of these objects has been described in detail by Jencson et al. (2019). Regarding our new targets, AT2016jbu and SN 2017jfs have been observed at only one epoch, while SN Hunt248—captured in total four times—shows a nearly constant, relatively blue color between 136 and 360 days.

3.3. A Comprehensive Multiwavelength Overview of LCs of Interacting SNe

Beyond the mid-IR, signs of ongoing circumstellar interaction can be most efficiently detected and traced in the form of radio, X-ray, or Hα emission. Fox et al. (2011) proposed a scenario whereby pre-shocked dust shells are radiatively heated by ongoing shock interaction at the inner radii, but the exact relationship between the different wavelengths may not be straightforward. Long-term multiwavelength monitoring, however, is quite limited; see recent reviews by Chevalier & Fransson (2017) and Chandra (2018), as well as (for example) Weiler et al. (2002), Dwarkadas & Gruszko (2012), and Vinkó et al. (2017) regarding radio, X-ray, and Hα data, respectively.

Figures 6 and 7, and Table 4, show an overview of long-term multiwavelength (radio, X-ray, Hα, near-IR, and mid-IR) LC evolution of many SNe in our sample (as well as Figure 8, zooming into the early-time evolution of SNe 2010jl and 2015da; see discussion below). While there are still only a few objects with well-sampled multichannel data sets, some conclusions can be drawn.

First, from the limited data available, near-IR and mid-IR LCs appear to have qualitatively similar evolution, particularly in the *K* band, which suggests that the dominant source of the detected flux at these wavelengths is the same—thermal continuum emission and not line emission. The availability of instruments with access to wavelengths longer than ∼2 μm is expected to be limited for high-cadence follow-up observations of transient objects in the near-term post-Spitzer era. Long-term near-IR (*K*-band) observations can be useful for monitoring the late-time evolution of the hottest dust when long-wavelength observations are unavailable. This could be particularly useful during the upcoming era of the Nancy Grace Roman Space Telescope (NGRST), which will be usable for similar follow-up observations of SNe (its longest-wavelength filter, F184, covers 1.68–2.00 μm, falling between the traditional *H* and *K* bands). We note, however, that the fundamental vibrational overtones of CO may contribute to not only 4.5 μm but also *K*-band fluxes of certain SNe (see, e.g., Jencson et al. 2017, 2019).

Furthermore, the average brightness levels of the objects seem to correlate with each other in every wavelength range (except radio). Dwarkadas & Gruszko (2012) and Ross & Dwarkadas (2017) published a compilation of X-ray LCs of different types of SNe, and their comparative figures show similarities to our mid-IR LC compilation (Figure 2) from the viewpoint that (some) SNe IIn represent the brightest sources, while observed luminosities of other SNe scatter over a wide

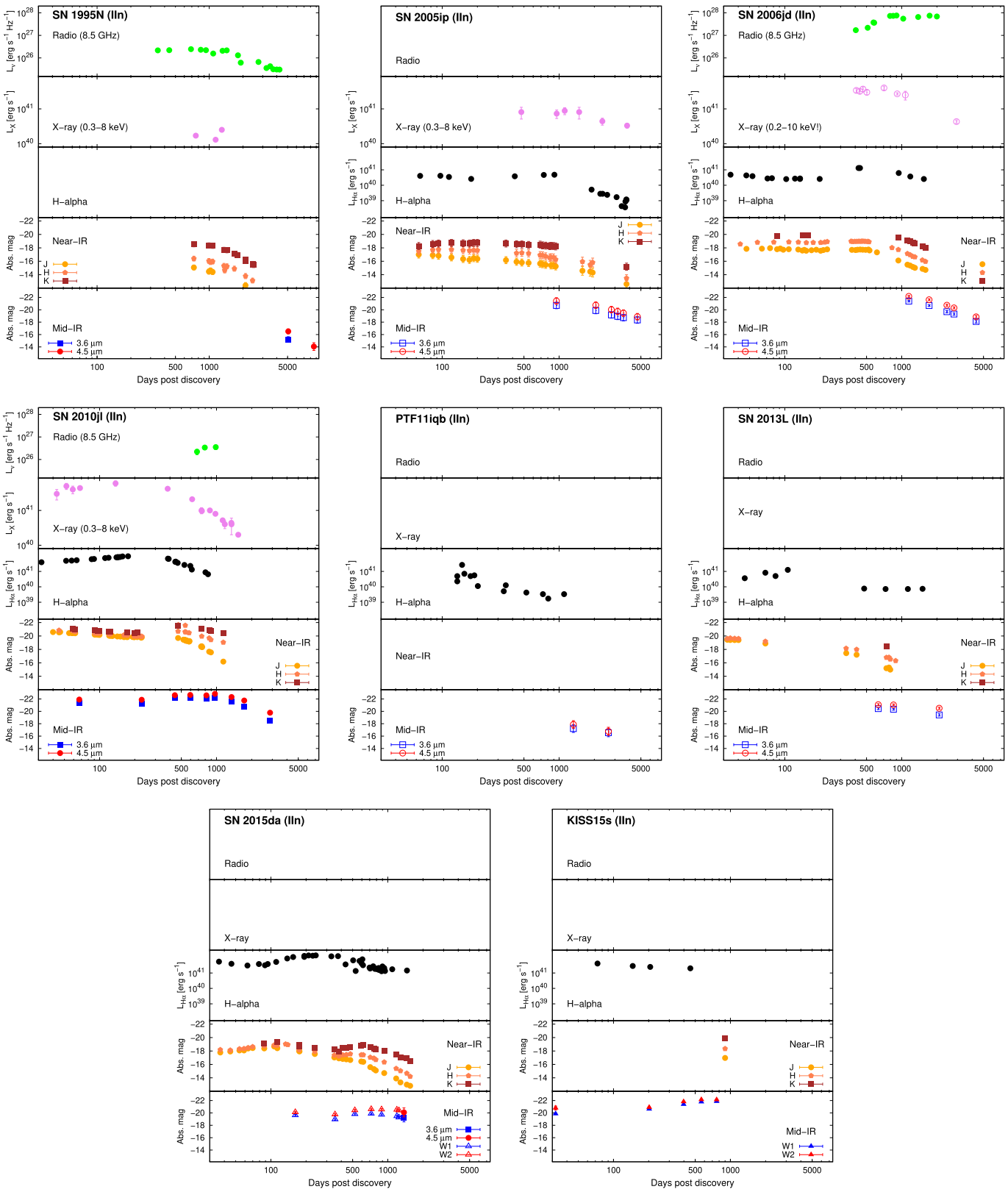

Figure 6. Comparative figures showing multiwavelength LCs of SNe IIn; sources of data are shown in Table 4. Regarding mid-IR data, circles/squares and triangles denote Spitzer and NEOWISE data, respectively; filled and empty symbols denote values determined with or without background subtraction, respectively. Regarding X-ray data, filled circles denote unabsorbed luminosities measured in the 0.3–8 keV regime, while empty circles denote values covering larger energy ranges.

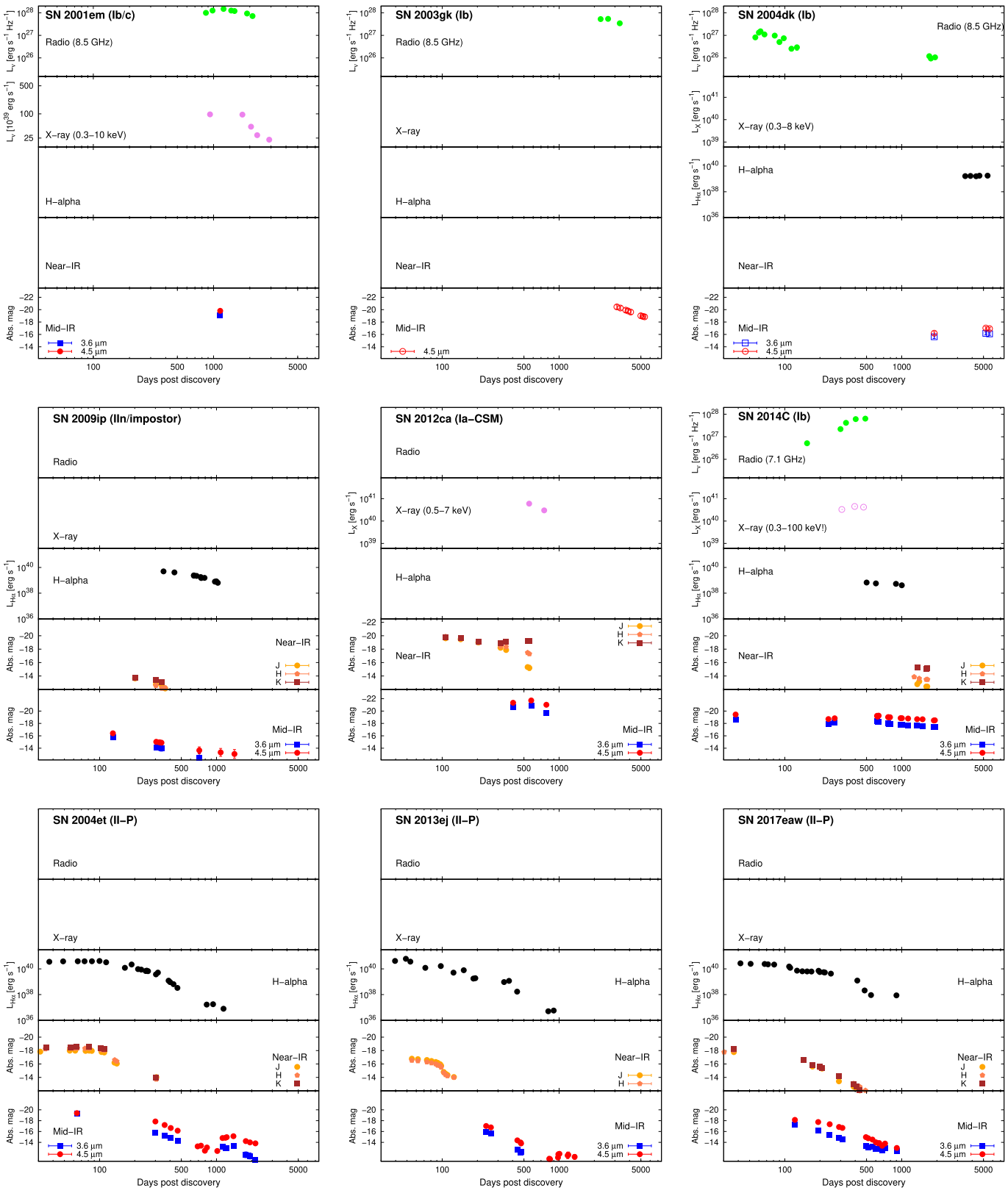

Figure 7. Comparative figures showing multiwavelength LCs of further late-time interacting SNe; sources of data are shown in Table 4. Regarding mid-IR data, filled and empty symbols denote values determined with or without image subtraction, respectively. Regarding X-ray data, filled circles denote unabsorbed luminosities measured in the 0.3–8 keV regime, while empty circles denote values covering larger energy ranges.

Table 4
Presence of Late-time Multiwavelength Data Sets for LASTCHANCE Targets and Other Interacting SNe

Object	Mid-IR	Near-IR	Hα flux	X-Ray	Radio	Refs.
IIn						
SN 1995N	Yes	Yes	⋯	Yes	Yes	1–9
SN 2005ip	Yes	Yes	Yes	Yes	Yes	1, 10–16
SN 2006jd	Yes	Yes	Yes	Yes	Yes	1, 13, 16, 17
SN 2010jl	Yes	Yes	Yes	Yes	Yes	1, 16, 18–21
PTF11iqb	Yes	⋯	Yes	⋯	⋯	1, 22, 23
SN 2013L	Yes	Yes	Yes	⋯	⋯	1, 24, 25
SN 2015da	Yes	Yes	Yes	⋯	⋯	1, 26
KISS15s	Yes	Yes	Yes	⋯	⋯	27
IIn/impost.						
SN 2009ip	Yes	Yes	Yes	⋯	⋯	1, 16, 23, 28–30
Ib/c						
SN 2001em	Yes	⋯	⋯	Yes	Yes	1, 16, 31–36
SN 2003gk	Yes	⋯	⋯	⋯	Yes	1, 37
SN 2004dk	Yes	⋯	Yes	⋯	Yes	1, 23, 38–40
SN 2014C	Yes	Yes	Yes	Yes	Yes	39, 41–44
Ia-CSM						
SN 2012ca	Yes	Yes	⋯	Yes	⋯	1, 16, 45–47
SN 2013dn	Yes	Yes	⋯	⋯	⋯	16, 45
II-P						
SN 2004et	Yes	Yes	Yes	⋯	⋯	48–51
SN 2013ej	Yes	Yes	Yes	⋯	⋯	16, 51–53
SN 2017eaw	Yes	Yes	Yes	⋯	⋯	1, 51, 54, 55

Notes. References: [1]This work; [2]Fox et al. (2000); [3]Fransson et al. (2002); [4]Gerardy et al. (2002); [5]Zampieri et al. (2005); [6]Chandra et al. (2005); [7]Chandra et al. (2009); [8]Pastorello et al. (2011); [9]Van Dyk (2013); [10]Fox et al. (2009); [11]Fox et al. (2010); [12]Fox et al. (2011); [13]Stritzinger et al. (2012); [14]Katsuda et al. (2014); [15]Smith et al. (2017); [16]Szalai et al. (2019a); [17]Chandra et al. (2012); [18]Andrews et al. (2011a); [19]Fransson et al. (2014); [20]Chandra et al. (2015); [21]Katsuda et al. (2016); [22]Smith et al. (2015); [23]Mauerhan et al. (2018a); [24]Andrews et al. (2017); [25]Taddia et al. (2020); [26]Tartaglia et al. (2020); [27]Kokubo et al. (2019); [28]Graham et al. (2014); [29]Fraser et al. (2015); [30]Graham et al. (2017); [31]Pooley (2007); [32]Stockdale et al. (2007); [33]Kelley et al. (2007); [34]Bietenholz & Bartel (2007); [35]Schinzel et al. (2009); [36]Chandra et al. (2020); [37]Bietenholz et al. (2014); [38]Wellons et al. (2012); [39]Vinkó et al. (2017); [40]Pooley et al. (2019); [41]Tinyanont et al. (2016); [42]Margutti et al. (2017); [43]Tinyanont et al. (2019b); [44]Bietenholz et al. (2018); [45]Fox et al. (2015); [46]Inserra et al. (2016); [47]Bochenek et al. (2018); [48]Kotak et al. (2009); [49]Fabbri et al. (2011); [50]Maguire et al. (2010); [51]Weil et al. (2020); [52]Mauerhan et al. (2017); [53]Dhungana et al. (2016); [54]Tinyanont et al. (2019a); [55]Szalai et al. (2019b).

range. In the near-IR and Hα, one can also see similar trends. Nevertheless, it is important to note that, at this time, lack of data imposes strong limitations on a more detailed comparative analysis, especially in the cases of non-SN IIn interacting SNe.

A further purpose of our current study has been to find any direct correlation between long-term X-ray/Hα and mid-IR LC evolution, which has been poorly studied to date in the literature. While comparative analyses of long-term X-ray, radio, Hα, optical, and near-IR SN LCs were published in several cases (see, e.g., Stritzinger et al. 2012; Fransson et al. 2014; Chandra et al. 2015), mid-IR LCs have not usually been (directly) involved in these comparisons.

A famous exception is the very nearby SN 1987A, for which the most complete long-term multiwavelength mid-IR/X-ray data sets were published (Bouchet et al. 2006; Dwek et al. 2010; Arendt et al. 2016). Only in this case can both very well-sampled mid-IR (from 3.6 to 24 μm) and X-ray evolution of an SN be followed for several thousand days, unfolding the ongoing interaction of the SN blast wave with a pre-existing dusty equatorial ring. In the listed papers, the IR-to-X-ray flux ratio (IRX) has been applied for investigating the process of gas–grain collisions and cooling of the shocked gas. As a shock sweeps though a medium with pre-existing dust, the IRX (at these mid-IR wavelengths) would be expected to decline as collisionally heated dust cools or is destroyed by sputtering. An epoch of dust formation in a CDS could act to increase the IRX, as could radiative processes (heating of the dust), in which case there is no direct physical interpretation of the IRX. However, we note that the level of mid-IR activity measured in SN 1987A is far below the detection limit of Spitzer for the more distant extragalactic SNe, maybe because the CSM forms a ring rather than a shell in SN 1987A (however, even these low fluxes could be available for JWST).

Another example is the Type IIn SN 2005ip, which has also been monitored for quite a long time (∼1000–5000 days; Fox et al. 2020). The mid-IR and (soft) X-ray (Katsuda et al. 2014; Smith et al. 2017) LCs seem to follow similarly decreasing trends, in agreement with the scenario that the primary source of the observed mid-IR flux is warm dust radiatively heated by energetic photons emerging from CSM interaction, and that the shock may be finally reaching the outer extent of the dense CSM shell. The multiwavelength evolution, including Hα, shows a shape that resembles that of an unabsorbed X-ray LC (see Smith et al. 2017, and also Figure 6). SN 2006jd, another

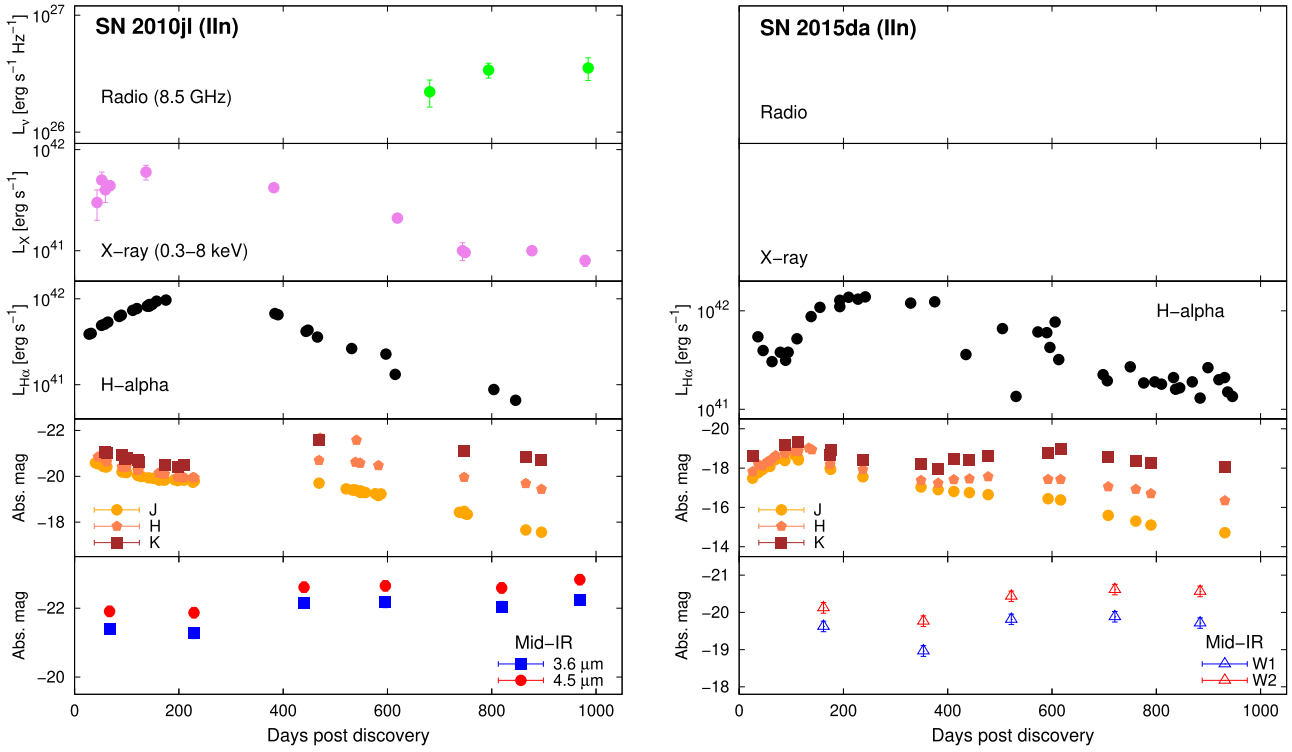

Figure 8. The same as in Figure 6, but using a linear timescale and zoomed-in to the first ∼1000 days of SN 2010jl (left) and SN 2015da (right).

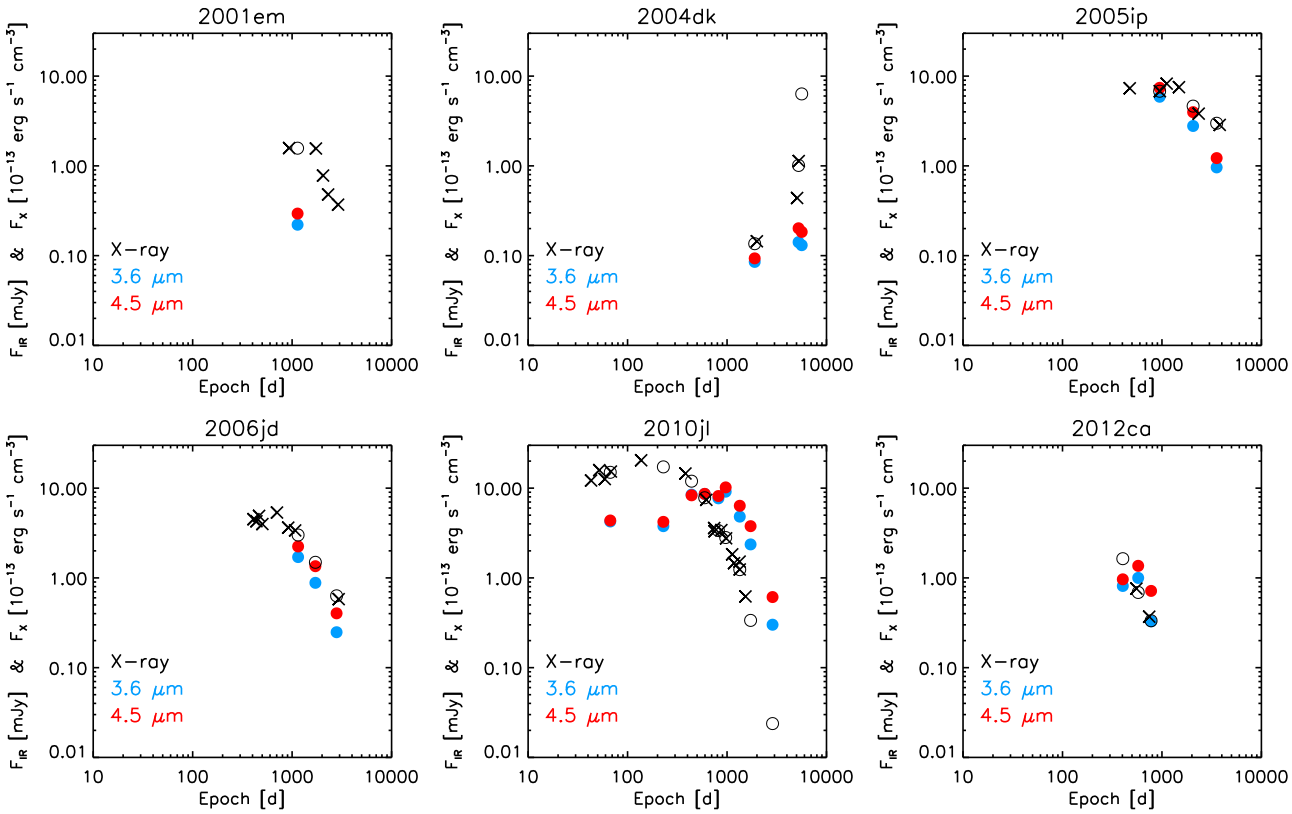

Figure 9. Comparative evolution of X-ray and mid-IR fluxes of interacting SNe from our sample. Black circles indicate the X-ray fluxes interpolated to the epochs of the mid-IR observations.

SN IIn, shows a quite similar behavior to that of SN 2005ip at various wavelengths; however, there is a lack of data after ∼2000 days (except in the mid-IR).

Based on the results of the first extended Spitzer survey of interacting SNe, Fox et al. (2013) also presented figures summarizing parallel mid-IR, X-ray, and optical (*R*-band)

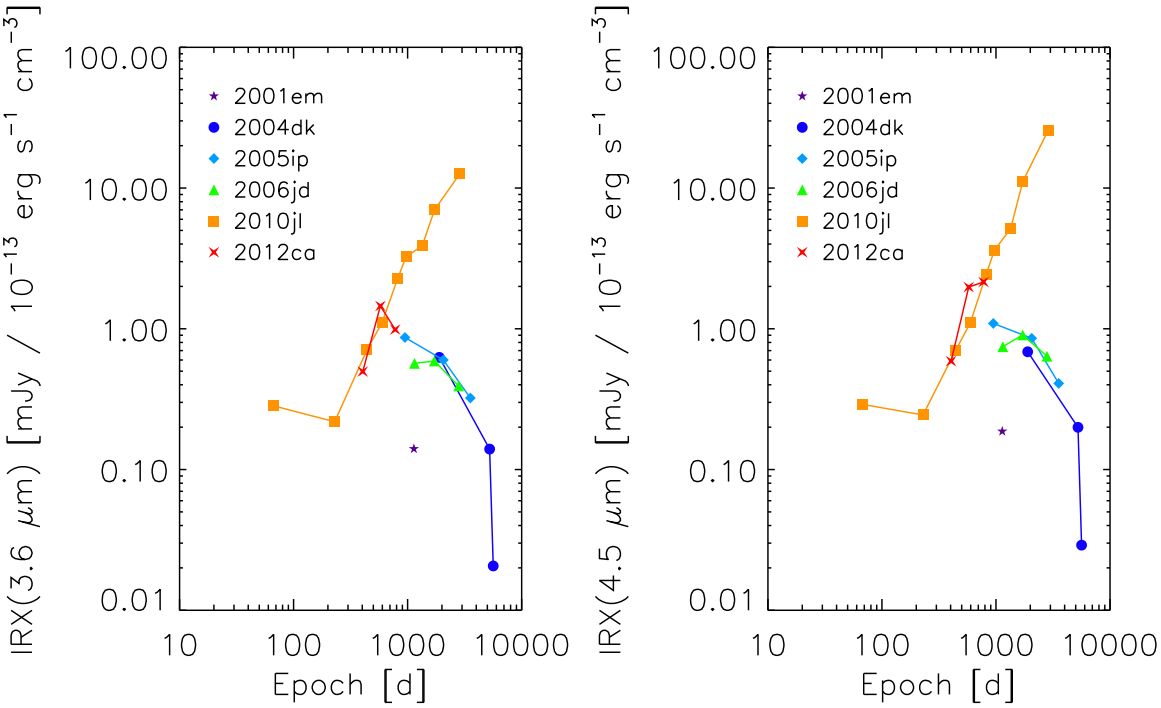

Figure 10. IRX ratios for SNe presented in Figure 9.

evolution of several SNe IIn; however, most of those LCs consist of only very few points.

In order to map similar correlations in our sample, we plotted the parallel evolution of all six SNe where both mid-IR and X-ray fluxes are available, and also calculated the IRX ratios for these objects (see Figures 9 and 10). Unfortunately, the amount and sampling of these data allow us to make only a preliminary analysis. Based on that, it seems that in SNe 2004dk, 2005ip, and 2006jd (expected to have radiatively heated pre-existing dust in their environments), all wavelengths trace each other (as proposed by, e.g., Fox et al. 2011).

While in most cases, comparative analysis of mid-IR and X-ray data was possible at epochs after ∼1000 days, it would be very interesting to see similar analyses at earlier phases. The only object with well-sampled mid-IR and X-ray data before ∼1000 days is the Type IIn SN 2010jl (see Figures 6 and 8–10). While SN 2010jl exhibits near-IR and mid-IR rebrightening and a quite long plateau after ∼400 days, it is preceded by an X-ray/Hα peak somewhere between 200 and 300 days. As previously noted (e.g., Fransson et al. 2014; Gall et al. 2014; Sarangi et al. 2018; Bevan et al. 2020), an IR excess before ∼400 days may be the consequence of heating of pre-existing dust, while mid-IR flux at a later time may originate either from new dust in the CDS and/or the ejecta or from CSM dust. Sarangi et al. (2018) presented a comparative analysis of mid-IR and X-ray LCs, and we complete that comparison here with the addition of an Hα LC (adopted from Fransson et al. 2014).

If we take into account general similarities between mid-IR and near-IR and between X-ray and Hα (see above), we can also find some further cases where early-time multiwavelength evolution can be well traced. Two other SNe IIn, SN 2015da (Tartaglia et al. 2020) and KISS15s (Kokubo et al. 2019), also show mid-IR LC evolution similar to that of SN 2010jl in the first ∼1000 days (up to the end of their data sets), probably going through similar circumstellar and dust-formation processes. In the case of SN 2015da, this is also strengthened by the parallel evolution of Hα and mid-IR luminosities (Figure 8 (right panel), adapted from Tartaglia et al. 2020).

In SNe IIn 2005ip and 2006jd, one can see long plateaus in both the near-IR and X-ray/Hα ranges during the first several hundred days, in accordance with their later-time LCs also tracing each other (as described above).

There are also well-sampled near-IR/mid-IR and Hα LCs of the Type II-P SNe 2004et and 2017eaw and of the Type II-P/L SN 2013ej (see Figure 7). These LCs trace each other quite well, during both their declining and their small rebrightening phases (the latter ones can be seen at ∼800–1000 days). This can be explained well by CDS dust formation described in Section 3.1.4.

As a conclusion of this part, our preliminary studies show that comparative analysis of long-term multiwavelength (especially X-ray/Hα versus mid-IR) data sets is an essential (and maybe the only really useful) tool to differentiate between the existing dust forming and heating scenarios and thus to get a complete picture of the physical processes going on in the circumstellar environments of interacting SNe. We plan to carry out a more detailed investigation of this topic, expecting high-quality data in the near future (e.g., from approved JWST and associated programs).

4. Conclusion

Here we have presented new Spitzer (3.6 and 4.5 μm) photometry of 19 interacting SNe from various classes (18 of them observed during our LASTCHANCE survey), together with some nondetections. We also collected all previously published data for studying the long-term mid-IR evolution of these objects and for revealing the origin of this IR excess (which can be observed for thousands of days in certain cases).

We can draw some conclusions regarding every studied type of interacting SN. Assuming that the main source of mid-IR

luminosity of SNe IIn is pre-existing dust, the mid-IR brightness evolution of these objects further confirms the presence of extended dense CSM in their close environments. At the same time, in most cases, very late-time ($\gtrsim$2000 days) mid-IR fluxes continuously decrease, indicating that CSM interaction ultimately weakens, possibly at a predictable rate.

The detected, homogeneous mid-IR evolution may hint that SNe Ia-CSM explode in very similar environments surrounded by dense but less extended CSM than SNe IIn do. While further data are necessary to reveal the true nature of SN Ia-CSM explosions, the presented mid-IR LCs may hint that their progenitors form a homogeneous class (contrary to SNe IIn), which also can support their thermonuclear origin. Mid-IR data on the stripped-envelope SNe in our sample support the idea that there can be detached CSM shells around some of these objects. Delayed CSM interaction may not begin for years, or even more than a decade, after explosion. Mid-IR properties of intermediate-luminosity interacting transients, just like their optical ones, are quite heterogeneous. These results support the assumption that either the progenitors, explosion mechanisms, or environmental circumstances of these objects may be quite different.

Comparison of long-term mid-IR LCs with those obtained in other wavelength ranges (especially X-ray, Hα, and near-IR) can be an efficient method to reveal otherwise hidden details of the connection between CSM interaction and formation/heating of ambient dust. Our analysis of multiwavelength data sets of SNe, especially regarding mid-IR versus X-ray luminosity evolution, supports previous results: some interacting SNe (such as SNe 2004dk, 2005ip, and 2006jd) seem to have large amounts of radiatively heated, slowly cooling pre-existing dust in their environments, while others (such as SN 2010jl, but probably also SN 2015da or KISS15s) exhibit signs of dust formation after explosion.

Our current study supports the idea that long-term mid-IR follow-up observations can play a key role in a better understanding of both pre- and post-explosion processes in exploding stars and in their environments. While Spitzer, the most effective tool that has been used for this purpose, is not available anymore, we have good prospects for the near future. Expected observations with JWST will have unique sensitivity to cooler dust grains at wavelengths $>4.5\,\mu$m and faint emission from SNe even years after explosion that would have gone undetected by Spitzer or any other mid-IR spacecraft. We also showed that, in dusty SNe, near-IR (K-band) LC evolution is quite similar to what we can see in the mid-IR. Thus, either ground-based or (upcoming) near-IR space telescopes (e.g., NGRST) can be effectively used for monitoring warm SN dust evolution, as well as in selecting appropriate targets for JWST and for other top-class IR telescopes in the future.

This work is based on observations made with the Spitzer Space Telescope, which was operated by the Jet Propulsion Laboratory, California Institute of Technology, under a contract with the National Aeronautics and Space Administration (NASA). Support for this work was provided by NASA through an award issued by JPL/Caltech. This research has made use of the NASA/IPAC Infrared Science Archive and NASA/IPAC Extragalactic Database (NED), which are both operated by JPL/Caltech, under contract with NASA; the SIMBAD database, operated at CDS, Strasbourg, France; the Supernova X-Ray Database (SNaX) funded by NASA Astrophysics Data Analysis program grant NNX14AR63G awarded to the University of Chicago; and the Open Supernova Catalog. We acknowledge the availability of the SAO/NASA Astrophysical Data System (ADS) services. This project has been supported by the GINOP-2-3-2-15-2016-00033 project of the National Research, Development and Innovation Office of Hungary (NKFIH) funded by the European Union, and by NKFIH/OTKA FK-134432 grant. T.S. is supported by the János Bolyai Research Scholarship of the Hungarian Academy of Sciences and by the New National Excellence Program (UNKP-20-5) of the Ministry for Innovation and Technology of Hungary from the source of the National Research, Development and Innovation Fund. A.V.F. is grateful for support from the U.C. Berkeley Miller Institute for Basic Research in Science (in which he is a Senior Miller Fellow), the TABASGO Foundation, the Christopher R. Redlich Fund, and many other individual donors. R.G.A. was supported by NASA under award number 80GSFC21M0002.

Facility: Spitzer(IRAC).

Software: IRAF.

ORCID iDs

Tamás Szalai https://orcid.org/0000-0003-4610-1117
Ori D. Fox https://orcid.org/0000-0003-2238-1572
Richard G. Arendt https://orcid.org/0000-0001-8403-8548
Eli Dwek https://orcid.org/0000-0001-8033-1181
Jennifer E. Andrews https://orcid.org/0000-0003-0123-0062
Geoffrey C. Clayton https://orcid.org/0000-0002-0141-7436
Alexei V. Filippenko https://orcid.org/0000-0003-3460-0103
Joel Johansson https://orcid.org/0000-0001-5975-290X
A. P. Marston https://orcid.org/0000-0001-5788-5258
Jon C. Mauerhan https://orcid.org/0000-0002-7555-8741
Schuyler D. Van Dyk https://orcid.org/0000-0001-9038-9950

References

Andrews, J. E., Clayton, G. C., Wesson, R., et al. 2011a, AJ, 142, 45
Andrews, J. E., Gallagher, J. S., Clayton, G. C., et al. 2010, ApJ, 715, 541
Andrews, J. E., Smith, N., McCully, C., et al. 2017, MNRAS, 471, 4047
Andrews, J. E., Sugerman, B. E. K., Clayton, G. C., et al. 2011b, ApJ, 731, 47
Arendt, R. G., Dwek, E., Bouchet, P., et al. 2016, AJ, 151, 62
Arendt, R. G., Dwek, E., Bouchet, P., et al. 2020, ApJ, 890, 2
Balam, D. 2017, TNSCR, 2017-880, 1
Balanutsa, P., & Lipunov, V. 2011, CBET, 2826, 1
Berton, M., Bufano, F., Floers, A., et al. 2018, ePESSTO Transient Classification Report for 2018-01-05, 2018-14
Bevan, A. M., Krafton, K., Wesson, R., et al. 2020, ApJ, 894, 111
Bietenholz, M. F., & Bartel, N. 2007, ApJL, 665, L47
Bietenholz, M. F., De Colle, F., Granot, J., Bartel, N., & Soderberg, A. M. 2014, MNRAS, 440, 821
Bietenholz, M. F., Kamble, A., Margutti, R., Milisavljevic, D., & Soderberg, A. 2018, MNRAS, 475, 1756
Blagorodnova, N., Kotak, R., Polshaw, J., et al. 2017, ApJ, 834, 107
Bochenek, C. D., Dwarkadas, V. V., Silverman, J. M., et al. 2018, MNRAS, 473, 336
Bode, M. F., & Evans, A. 1980, MNRAS, 193, 21P
Bond, H. E., Bedin, L. R., Bonanos, A. Z., et al. 2009, ApJL, 695, L154
Bouchet, P., Dwek, E., Danziger, J., et al. 2006, ApJ, 650, 212
Brennan, S. J., Fraser, M., Johansson, J., et al. 2021a, arXiv:2102.09572
Brennan, S. J., Fraser, M., Johansson, J., et al. 2021b, arXiv:2102.09576
Brimacombe, J., Bock, G., Fernandez, J. M., et al. 2017, ATel, 10463, 1
Cartier, R., Sullivan, M., Firth, R. E., et al. 2017, MNRAS, 464, 4476
Chandra, P. 2018, SSRv, 214, 27
Chandra, P., Chevalier, R. A., Chugai, N., et al. 2012, ApJ, 755, 110

Chandra, P., Chevalier, R. A., Chugai, N., Fransson, C., & Soderberg, A. M. 2015, ApJ, 810, 32
Chandra, P., Chevalier, R. A., Chugai, N., Milisavljevic, D., & Fransson, C. 2020, ApJ, 902, 55
Chandra, P., Ray, A., Schlegel, E. M., Sutaria, F. K., & Pietsch, W. 2005, ApJ, 629, 933
Chandra, P., Stockdale, C. J., Chevalier, R. A., et al. 2009, ApJ, 690, 1839
Chevalier, R. A., & Fransson, C. 2017, Thermal and Non-thermal Emission from Circumstellar Interaction (Berlin: Springer), 875
Chugai, N. N., & Chevalier, R. A. 2006, ApJ, 641, 1051
Dhungana, G., Kehoe, R., Vinko, J., et al. 2016, ApJ, 822, 6
Dong, S., Bersier, D., & Prieto, J. L. 2017, ASAS-SN Transient Classification Report for 2017-10-11, 2017-1103
Drescher, C., Parker, S., & Brimacombe, J. 2012, CBET, 3101, 1
Dwarkadas, V. V., & Gruszko, J. 2012, MNRAS, 419, 1515
Dwek, E. 1983, ApJ, 274, 175
Dwek, E., & Arendt, R. G. 2008, ApJ, 685, 976
Dwek, E., Arendt, R. G., Bouchet, P., et al. 2010, ApJ, 722, 425
Fabbri, J., Otsuka, M., Barlow, M. J., et al. 2011, MNRAS, 418, 1285
Fazio, G. G., Hora, J. L., Allen, L. E., et al. 2004, ApJS, 154, 10
Fox, D. W., Lewin, W. H. G., Fabian, A., et al. 2000, MNRAS, 319, 1154
Fox, O., Skrutskie, M. F., Chevalier, R. A., et al. 2009, ApJ, 691, 650
Fox, O. D., Chevalier, R. A., Dwek, E., et al. 2010, ApJ, 725, 1768
Fox, O. D., Chevalier, R. A., Skrutskie, M. F., et al. 2011, ApJ, 741, 7
Fox, O. D., & Filippenko, A. V. 2013, ApJL, 772, L6
Fox, O. D., Filippenko, A. V., Skrutskie, M. F., et al. 2013, AJ, 146, 2
Fox, O. D., Fransson, C., Smith, N., et al. 2020, MNRAS, 498, 517
Fox, O. D., Silverman, J. M., Filippenko, A. V., et al. 2015, MNRAS, 447, 772
Fransson, C., Chevalier, R. A., Filippenko, A. V., et al. 2002, ApJ, 572, 350
Fransson, C., Ergon, M., Challis, P. J., et al. 2014, ApJ, 797, 118
Fraser, M., Kotak, R., Pastorello, A., et al. 2015, MNRAS, 453, 3886
Fraser, M., Pastorello, A., Cartier, R., et al. 2017, ATel, 9938, 1
Gall, C., Hjorth, J., & Andersen, A. C. 2011, A&ARv, 19, 43
Gall, C., Hjorth, J., Watson, D., et al. 2014, Natur, 511, 326
Gao, Y., & Solomon, P. M. 2004, ApJS, 152, 63
Gerardy, C. L., Fesen, R. A., Nomoto, K., et al. 2002, ApJ, 575, 1007
Graham, J. R., & Meikle, W. P. S. 1986, MNRAS, 221, 789
Graham, M. L., Harris, C. E., Fox, O. D., et al. 2017, ApJ, 843, 102
Graham, M. L., Sand, D. J., Valenti, S., et al. 2014, ApJ, 787, 163
Guillochon, J., Parrent, J., Kelley, L. Z., & Margutti, R. 2017, ApJ, 835, 64
Holoien, T. W. S., Prieto, J. L., Kochanek, C. S., et al. 2014, ATel, 6436, 1
Howell, D. A., & Murray, D. 2012, CBET, 3313, 2
Indebetouw, R., Matsuura, M., Dwek, E., et al. 2014, ApJL, 782, L2
Inserra, C., Fraser, M., Smartt, S. J., et al. 2016, MNRAS, 459, 2721
Inserra, C., Smartt, S. J., Valenti, S., et al. 2012, CBET, 3101, 1
Itagaki, K. 2017, Transient Discovery Report for 2017-01-11, 2017-44
Jencson, J. E., Kasliwal, M. M., Adams, S. M., et al. 2018, ApJ, 863, 20
Jencson, J. E., Kasliwal, M. M., Adams, S. M., et al. 2019, ApJ, 886, 40
Jencson, J. E., Kasliwal, M. M., Johansson, J., et al. 2017, ApJ, 837, 167
Jin, Z., Gao, X., McCully, C., & Jha, S. W. 2013, CBET, 3520, 1
Johansson, J., Goobar, A., Kasliwal, M. M., et al. 2017, MNRAS, 466, 3442
Kasliwal, M. M., Bally, J., Masci, F., et al. 2017, ApJ, 839, 88
Katsuda, S., Maeda, K., Bamba, A., et al. 2016, ApJ, 832, 194
Katsuda, S., Maeda, K., Nozawa, T., Pooley, D., & Immler, S. 2014, ApJ, 780, 184
Kelley, M. T., Stockdale, C. J., Weiler, K. W., et al. 2007, in AIP Conf. Ser., 937, Supernova 1987A: 20 Years After: Supernovae and Gamma-Ray Bursters, ed. S. Immler, K. Weiler, & R. McCray (Melville, NY: AIP), 269
Kilpatrick, C. D., Coulter, D. A., Foley, R. J., Pan, Y. C., & Siebert, M. R. 2018, ATel, 11172, 1
Kochanek, C. S. 2011, ApJ, 741, 37
Kokubo, M., Mitsuda, K., Morokuma, T., et al. 2019, ApJ, 872, 135
Kollmeier, J. A., Chen, P., Dong, S., et al. 2019, MNRAS, 486, 3041
Kostrzewa-Rutkowska, Z., Benetti, S., Dong, S., et al. 2017, ATel, 10834, 1
Kotak, R., Meikle, P., van Dyk, S. D., Höflich, P. A., & Mattila, S. 2005, ApJL, 628, L123
Kotak, R., Meikle, W. P. S., Farrah, D., et al. 2009, ApJ, 704, 306
Kozasa, T., Nozawa, T., Tominaga, N., et al. 2009, in ASP Conf. Ser., 414, Cosmic Dust—Near and Far, ed. T. Henning, E. Grün, & J. Steinacker (San Francisco, CA: ASP), 43
Kumar, B., Eswaraiah, C., Singh, A., et al. 2019, MNRAS, 488, 3089
Lin, H., Li, W., Wang, X., et al. 2018, ATel, 11393, 1
Maguire, K., Di Carlo, E., Smartt, S. J., et al. 2010, MNRAS, 404, 981
Margutti, R., Kamble, A., Milisavljevic, D., et al. 2017, ApJ, 835, 140
Margutti, R., Milisavljevic, D., Soderberg, A. M., et al. 2014, ApJ, 780, 21
Matsuura, M., Dwek, E., Barlow, M. J., et al. 2015, ApJ, 800, 50
Matsuura, M., Dwek, E., Meixner, M., et al. 2011, Sci, 333, 1258
Mattila, S., Meikle, W. P. S., Lundqvist, P., et al. 2008, MNRAS, 389, 141
Mauerhan, J. C., Filippenko, A. V., Brink, T. G., & Zheng, W. 2017, ATel, 10911, 1
Mauerhan, J. C., Filippenko, A. V., Zheng, W., et al. 2018a, MNRAS, 478, 5050
Mauerhan, J. C., Van Dyk, S. D., Graham, M. L., et al. 2015, MNRAS, 447, 1922
Mauerhan, J. C., Van Dyk, S. D., Johansson, J., et al. 2018b, MNRAS, 473, 3765
Meikle, W. P. S., Kotak, R., Farrah, D., et al. 2011, ApJ, 732, 109
Meikle, W. P. S., Mattila, S., Pastorello, A., et al. 2007, ApJ, 665, 608
Milisavljevic, D., Margutti, R., Kamble, A., et al. 2015, ApJ, 815, 120
Ofek, O. 2012, CBET, 3313, 1
Papenkova, M., Li, W. D., Wray, J., Chleborad, C. W., & Schwartz, M. 2001, IAU Circ., 7722, 1
Parrent, J., Levitan, D., Howell, A., et al. 2011, ATel, 3510, 1
Pastorello, A., Benetti, S., Bufano, F., et al. 2011, AN, 332, 266
Pastorello, A., Chen, T. W., Cai, Y. Z., et al. 2019a, A&A, 625, L8
Pastorello, A., Mason, E., Taubenberger, S., et al. 2019b, A&A, 630, A75
Pooley, D. 2007, in AIP Conf. Ser., 937, Supernova 1987A: 20 Years After: Supernovae and Gamma-Ray Bursters, ed. S. Immler, K. Weiler, & R. McCray (Melville, NY: AIP), 381
Pooley, D., & Lewin, W. H. G. 2004, IAU Circ., 8323, 2
Pooley, D., Wheeler, J. C., Vinkó, J., et al. 2019, ApJ, 883, 120
Pozzo, M., Meikle, W. P. S., Fassia, A., et al. 2004, MNRAS, 352, 457
Prieto, J. L. 2011, CBET, 2826, 2
Prieto, J. L., Kistler, M. D., Thompson, T. A., et al. 2008, ApJL, 681, L9
Reach, W. T., Rho, J., Tappe, A., et al. 2006, AJ, 131, 1479
Reilly, E., Maund, J. R., Baade, D., et al. 2017, MNRAS, 470, 1491
Ross, M., & Dwarkadas, V. V. 2017, AJ, 153, 246
Sarangi, A., Dwek, E., & Arendt, R. G. 2018, ApJ, 859, 66
Schinzel, F. K., Taylor, G. B., Stockdale, C. J., Granot, J., & Ramirez-Ruiz, E. 2009, ApJ, 691, 1380
Schlegel, E. M. 1990, MNRAS, 244, 269
Silverman, J. M., Nugent, P. E., Gal-Yam, A., et al. 2013, ApJS, 207, 3
Siviero, A., Tomasella, L., Pastorello, A., et al. 2012, CBET, 3054, 4
Smith, N. 2017, Interacting Supernovae: Types IIn and Ibn (Berlin: Springer), 403
Smith, N., & Andrews, J. E. 2020, MNRAS, 499, 3544
Smith, N., Kilpatrick, C. D., Mauerhan, J. C., et al. 2017, MNRAS, 466, 3021
Smith, N., Mauerhan, J. C., Cenko, S. B., et al. 2015, MNRAS, 449, 1876
Soderberg, A. M., Gal-Yam, A., & Kulkarni, S. R. 2004, GCN, 2586, 1
Sorce, J. G., Tully, R. B., Courtois, H. M., et al. 2014, MNRAS, 444, 527
Springob, C. M., Masters, K. L., Haynes, M. P., Giovanelli, R., & Marinoni, C. 2009, ApJS, 182, 474
Stockdale, C. J., Kelley, M. T., Weiler, K. W., et al. 2007, in AIP Conf. Ser., 937, Supernova 1987A: 20 Years After: Supernovae and Gamma-Ray Bursters, ed. S. Immler, K. Weiler, & R. McCray (Melville, NY: AIP), 264
Stockdale, C. J., Van Dyk, S. D., Sramek, R. A., et al. 2004, IAU Circ., 8282, 2
Stritzinger, M., Taddia, F., Fransson, C., et al. 2012, ApJ, 756, 173
Sugerman, B. E. K. 2003, AJ, 126, 1939
Sugerman, B. E. K., Ercolano, B., Barlow, M. J., et al. 2006, Sci, 313, 196
Szalai, T., & Vinkó, J. 2013, A&A, 549, A79
Szalai, T., Vinkó, J., Balog, Z., et al. 2011, A&A, 527, A61
Szalai, T., Vinkó, J., Könyves-Tóth, R., et al. 2019b, ApJ, 876, 19
Szalai, T., Zsíros, S., Fox, O. D., Pejcha, O., & Müller, T. 2019a, ApJS, 241, 38
Szczygieł, D. M., Kochanek, C. S., & Dai, X. 2012a, ApJ, 760, 20
Szczygieł, D. M., Prieto, J. L., Kochanek, C. S., et al. 2012b, ApJ, 750, 77
Taddia, F., Nyholm, A., Barbarino, C., et al. 2017, ATel, 10148, 1
Taddia, F., Stritzinger, M. D., Fransson, C., et al. 2020, A&A, 638, A92
Tartaglia, L., Pastorello, A., Sollerman, J., et al. 2020, A&A, 635, A39
Theureau, G., Hanski, M. O., Coudreau, N., Hallet, N., & Martin, J. M. 2007, A&A, 465, 71
Tinyanont, S., Kasliwal, M. M., Fox, O. D., et al. 2016, ApJ, 833, 231
Tinyanont, S., Kasliwal, M. M., Krafton, K., et al. 2019a, ApJ, 873, 127
Tinyanont, S., Lau, R. M., Kasliwal, M. M., et al. 2019b, ApJ, 887, 75
Vallely, P. J., Fausnaugh, M., Jha, S. W., et al. 2019, MNRAS, 487, 2372
Van Dyk, S. D. 2013, AJ, 145, 118
Vinkó, J., Pooley, D., Silverman, J. M., et al. 2017, ApJ, 837, 62
Weil, K. E., Fesen, R. A., Patnaude, D. J., & Milisavljevic, D. 2020, ApJ, 900, 11

Weiler, K. W., Panagia, N., Montes, M. J., & Sramek, R. A. 2002, ARA&A, 40, 387
Wellons, S., Soderberg, A. M., & Chevalier, R. A. 2012, ApJ, 752, 17
Wenger, M., Ochsenbein, F., Egret, D., et al. 2000, A&AS, 143, 9
Wesson, R., Barlow, M. J., Matsuura, M., & Ercolano, B. 2015, MNRAS, 446, 2089
Williams, B. J., & Temim, T. 2017, Infrared Emission from Supernova Remnants: Formation and Destruction of Dust (Berlin: Springer), 2105
Zampieri, L., Mucciarelli, P., Pastorello, A., et al. 2005, MNRAS, 364, 1419
Zhang, J., & Wang, X. 2015, ATel, 6939, 1
Zhang, J., Xu, L., & Wang, X. 2018, ATel, 11379, 1